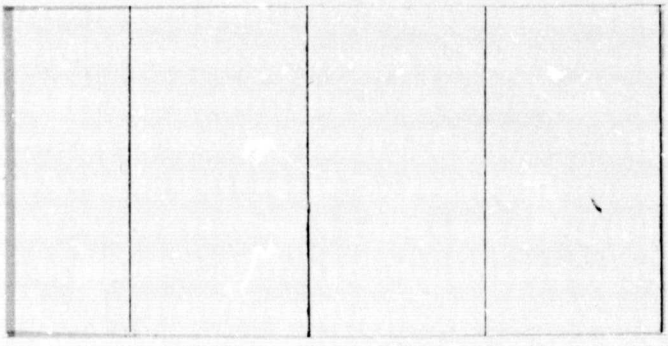

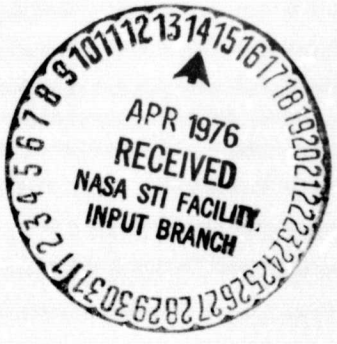

LOCKHEED
MISSILES & SPACE COMPANY, INC. • SUNNYVALE, CALIFORNIA
A SUBSIDIARY OF LOCKHEED AIRCRAFT CORPORATION

LMSC/D462625
7 November 1975

FINAL REPORT

STUDY OF PLASMASPHERE DYNAMICS USING INCOHERENT SCATTER DATA FROM CHATANIKA, ALASKA RADAR FACILITY

Contract NASw 2582

Prepared by

Dr. Edward G. Shelley
Principal Investigator
Space Sciences Laboratory
Lockheed Palo Alto Research Laboratory
LOCKHEED MISSILES & SPACE COMPANY, INC.
3251 Hanover Street
Palo Alto, California 94304

TABLE OF CONTENTS

FINAL REPORT
STUDY OF PLASMASPHERE DYNAMICS USING INCOHERENT SCATTER DATA FROM CHATANIKA, ALASKA RADAR FACILITY

Contract NASw 2582

Section 1
INTRODUCTION

This was a program for the cooperative study of Chatanika incoherent scatter radar data and Lockheed Palo Alto Research Laboratory (LPARL) satellite data. About 2/3 of the resources of the contract were utilized by LPARL and about 1/3 by the University of California at San Diego (UCSD) Computer Center and Prof. Peter M. Banks of UCSD who acted as a consultant for this program.

The principal results were in three separate areas. In the first area, we cooperated with T. M. Watt of the Stanford Research Institute (SRI) in a quantitative intercomparison of the precipitating electron fluxes measured over Chatanika, Alaska by the LPARL experiment on satellite 1971-89A and simultaneous electron density profiles obtained from the radar measurements. There was a large data base of simultaneous acquisitions from the two experiments during the period October 1971 through August 1972. These cases were examined and two examples were selected, with good coordination geometry, for detailed analysis. The results of this analysis have been published in the Journal of Geophysical Research and are given in Section 2 of this report.

In the second area we cooperated with Prof. Banks in qualitatively scanning a body of simultaneous radar and satellite data in a search for general morphological relationships. Survey plots from the 36 auroral particle detectors on satellite 1971-89A were prepared for 17 auroral zone traversals and scanned in conjunction with available electron density profiles and convection electric field measurements from Chatanika. Although no dramatic systematic

relationships between the two bodies of data were readily apparent, some interesting results did emerge from these intercomparisons and they are summarized in Sections 3 and 4 of this report.

In the third area we cooperated with R. T. Tsunoda of SRI and others in a joint study of data from a number of satellite and ground-based observatories, including Chatanika, during a single disturbed evening, on 21 March 1973. On this particular evening, in addition to the Lockheed satellite data and the Chatanika incoherent scatter results, there were also measurements available from the Homer, Alaska 398-MHz phased-array radar, a NASA barium ion cloud, a meridian chain of magnetometers and all-sky camera stations, and the field-aligned current experiment of the Johns Hopkins University, Applied Physics Laboratory, on the TRIAD satellite. The study of this large quantity of coordinated observations necessarily includes areas of interest outside the scope of this particular contract, and the study of these aspects of the data is being funded by other sources. Since the work in these other areas is not yet completed, a final paper is not yet available. A preliminary discussion and summary of some of the results is contained in Section 5 of this report.

VOL. 79, NO. 31 JOURNAL OF GEOPHYSICAL RESEARCH NOVEMBER 1, 1974
Page 4725

Section 2

Joint Radar-Satellite Determination of the Effective Recombination Coefficient in the Auroral *E* Region

T. M. WATT

Stanford Research Institute, Menlo Park, California 94025

L. L. NEWKIRK AND E. G. SHELLEY

Lockheed Palo Alto Research Laboratory, Palo Alto, California 94304

This paper reports on the experimental determination of the effective recombination coefficient α in the auroral *E* region. The technique consists of obtaining measurements, time coincident and nearly space coincident, of electron density from the Chatanika incoherent scatter radar and of electron production rate from the 1971-089A satellite. Electron density profiles are determined along the radar beam, and electron production profiles are field aligned. The horizontal separation caused by these and other factors can give rise to uncertainties in the presence of horizontal gradients in electron density or production. Values of α obtained by this technique are nevertheless in reasonable agreement with the results of others. Since the technique offers the possibility of frequent and routine determinations of α profiles (typically, four per day), it clearly represents a powerful means for providing synoptic studies of this ionospheric parameter.

At present there is a very high degree of interest in physical processes associated with the auroral ionosphere. In the *D* and *E* regions of the auroral ionosphere the parameter effective recombination coefficient α is of interest because of its relationship to electron-ion loss processes, and it is studied by a variety of techniques [*Biondi*, 1969; *Baron*, 1972; *Ulwick and Baron*, 1973].

The purpose of this paper is to present the results of a new technique to determine height profiles of α in the auroral *E* region. The technique combines height profiles of electron density from the Chatanika incoherent scatter radar [*Leadabrand et al.*, 1972] with coincident field-aligned profiles of electron production obtained from energetic particle measurements made by the 1971-089A satellite. Potentially, the power of this technique for synoptic studies of α is enormous in comparison with existing methods, since, in principle, a separate measurement can be made on every satellite pass occurring near the radar (typically, four per day).

In the *E* region the effects of negative ions can be neglected [*Biondi*, 1969]. If we also assume that plasma transport effects are negligible, then the steady state equation of continuity is given approximately by [*Rishbeth and Garriott*, 1969]

$$Q = \alpha N^2 = \{\alpha(NO^+)n(NO^+) + \alpha(O_2^+)n(O_2^+)\}N \quad (1)$$

from which it follows that

$$\alpha = Q/N^2 = [\alpha(NO^+)n(NO^+) + \alpha(O_2^+)n(O_2^+)]/N \quad (2)$$

where

Q electron production rate;
N electron number density;
$\alpha(X^+)$ recombination coefficient of ion species X^+;
$n(X^+)$ number density of ion species X^+;
α effective recombination coefficient.

In addition to its dependence on species and number density of ions, α is dependent on neutral density [*Poppoff and Whitten*, 1968] and is temperature sensitive [*Biondi*, 1969].

As is indicated in (2), α can be experimentally determined from the quotient Q/N^2. The efficacy of such a determination rests on obtaining time and space coincident measurements of electron production rate and electron number density.

At any instant of time the radar obtains a range profile of electron density along the antenna beam, and the satellite obtains an in situ measurement of the energy spectrum and pitch angle distribution of precipitating particles at the position of the satellite (~800-km altitude). The instantaneous measurement at the satellite can, by using an appropriate computer code, be transformed into an electron production profile along the geomagnetic field line [*Cain et al.*, 1967] passing through the satellite. The essence of the experiment is to coordinate the radar operation, both in time and in antenna pointing angle, to obtain an intersection between a radar-obtained density profile and a satellite-obtained production profile.

The best possible geometrical circumstance for a coordinated measurement would be that the satellite would pass through that geomagnetic field line occupied by the radar. The radar antenna beam could then be directed up the field line, and if the small amount of curvature in the field line is neglected, the production and density profiles would be congruent. Realistically, of course, this condition is never achieved, and in any actual measurement the field line profile of production and the antenna beam profile of density are skew with respect to each other and can intersect at only one place. When such skewness exists, a particular altitude must be chosen at which intersection is to take place.

INSTRUMENTATION

The Chatanika facility is an *L* band (1290 MHz) fully steerable incoherent scatter radar system located at 65.1°N, 147.45°W (L = 5.7) near Fairbanks, Alaska. The system has been described in considerable detail [*Leadabrand et al.*, 1972; *Baron*, 1972; *Watt*, 1973] and will not be described further here.

The 1971-089A satellite was in a nearly circular 93° inclination orbit at approximately 800 km. The satellite was three-axis stabilized and geocentrically oriented. The particle data utilized here were obtained from two sets of fixed energy detectors oriented at 15° and 55°, respectively, from the local zenith. The electron instruments consisted of 180° permanent

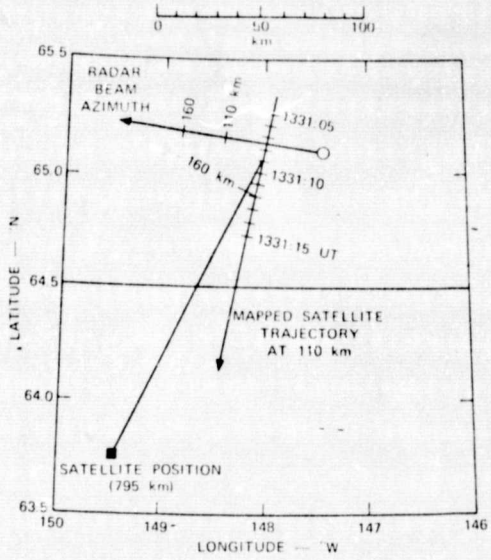

Fig. 1. Plan view geometry of the radar beam and the mapped trajectory of the satellite during the coordinated experiment on December 8, 1971.

magnet spectrometers with channeltron detectors. There were seven independent sensors at 15° and nine independent sensors at 55°. The instruments had contiguous energy passbands of $\Delta E/E$ between 0.60 and 1.10 and provided complete coverage of the electron fluxes from approximately 70 eV to 40 keV at both angles. The proton data used here were derived from integral flux detectors with proton thresholds at 16 and 39 keV at each of the two angles. These types of instruments have been described in more detail by *Shea et al.* [1967], *Reed et al.* [1969], and *Paschmann et al.* [1970].

The pulses from each sensor output were fed into a log count rate meter with a time constant of approximately 300 ms. The rate meters were sampled by the telemetry approximately 5 times per second. This analysis utilized one sample per second from each detector.

Experiment

During the period October 1971 through April 1972, several radar-satellite coordinated measurements were made, and these measurements comprise the data base for this study. At the time of these measurements, the radar was being operated according to other unrelated experiments, so that the radar antenna was not pointed so as to provide optimal coincidence with the satellite measurements.

From the total data base, two events, occurring at 1331 UT (0331 LST, 124° solar zenith angle) on December 8, 1971, and at 1114 UT (0114 LST, 132° solar zenith angle) on January 27, 1972, were selected for detailed analysis. The contrasting results of these two events demonstrate both the efficacy of the technique and certain limitations on quantitative conclusions.

The spatial criterion for the coordinated measurements is given by the requirement that at 110-km altitude, the radar beam and field-line-mapped position of the satellite lie on the same geomagnetic latitude. This coordination criterion is consistent with typical radar observations of auroral E ionization in which maximum electron densities occur near 100–120 km and latitudinal density gradients are much larger than longitudinal density gradients [*Baron*, 1972].

Figures 1 and 2 illustrate plan views of the two measurements plotted in geographic coordinates for December 8 and January 27, respectively. Each figure illustrates the mapped trajectory of the satellite at 110-km altitude, the projection of the radar beam and its location at 110-km altitude, and the point on the mapped trajectory corresponding to the geomagnetic latitude of the 110-km intersection of the radar beam.

It can be seen from the figures that, by our criterion, the optimal times for the coordinated measurements are 1331:09 UT on December 8 and 1114:12 UT on January 27 and the horizontal distances (at 110-km altitude) between the corresponding electron density and electron production measurements are about 21 and 18 km, respectively.

The measured data from both the radar and the satellite were integrated over finite times in order to reduce statistical fluctuations to acceptable levels. This requirement is illustrated for the radar measurements on December 8 and January 27 in Figures 3 and 4, respectively, which present for each case overlays of three electron density profiles obtained by the radar while the satellite was passing nearby. It can be seen that for these cases the electron density maximums occur near 110-km altitude. We can associate the large high-altitude fluctuations appearing in the 10-s or 20-s profiles with statistical noise fluctuations in the radar receiver; thus it is apparent that no large temporal variations in electron density are being observed during the 1-min periods on either December 8 or January 27. Accordingly, in order to provide valid electron density data relatively free from statistical noise effects, we take the 1-min electron density profiles as comprising the radar input to the coordinated measurements. In the altitude range below 150 km the standard deviation of statistical errors using a 1-min integration is estimated to be less than 8×10^3 el/cm^3.

As was pointed out in the previous section, a complete data set was obtained from the satellite instrumentation once per second. These particle data were then averaged over a period of 4 s, corresponding to a distance traveled along the mapped trajectory of about 28 km (see Figures 1 and 2).

Figures 5 and 6 illustrate the second-by-second outputs of two of the satellite-mounted electron sensors for time periods encompassing each of the two specific measurement times. The curves illustrate the differential electron flux in the energy

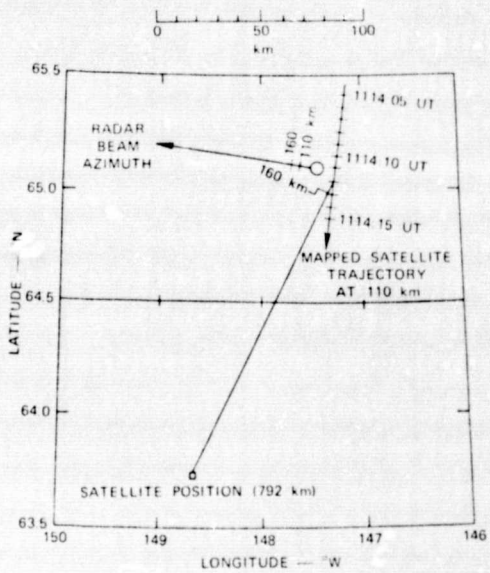

Fig. 2. Plan view geometry of the radar beam and the mapped trajectory of the satellite during the coordinated experiment on January 27, 1972.

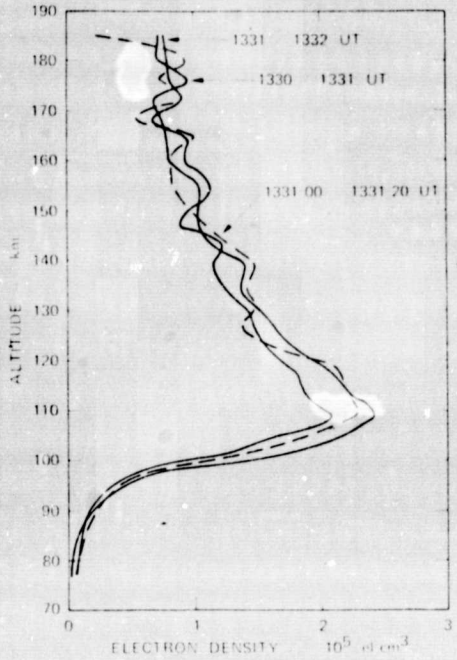

Fig. 3. Electron density profiles obtained from radar measurements during the coordinated radar-satellite experiment on December 8, 1971.

ranges indicated. These curves are representative of flux variations over the entire energy range measured. Representative statistical uncertainties associated with the measured values are indicated by the error bars.

The data for January 27 show a variation of much less than a factor of 2 over the 4-s period 1114:10 to 1114:14 UT. Aside from the small fluctuations present in the second-by-second data, the measured flux did not exhibit any significant latitudinal variation in the vicinity of Chatanika.

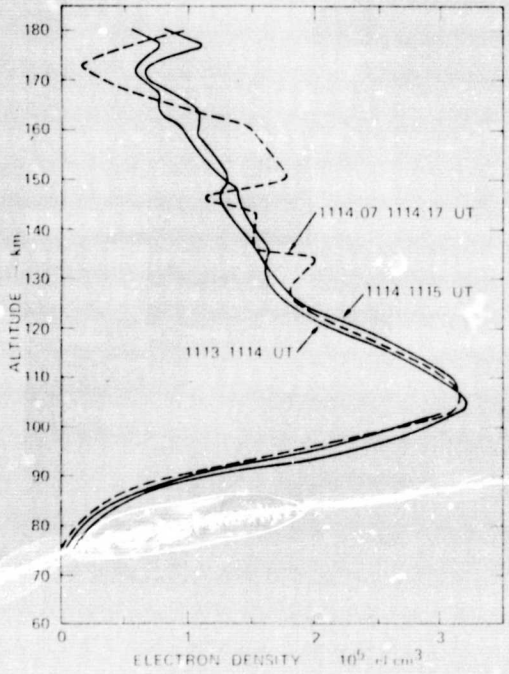

Fig. 4. Electron density profiles obtained from radar measurements during the coordinated radar-satellite experiment on January 27, 1972.

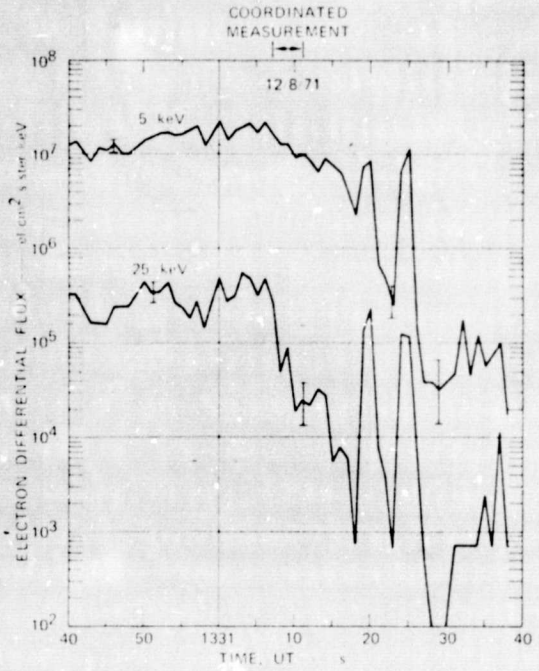

Fig. 5. Electron differential flux as a function of time for two satellite-mounted particle counters, centered at 5 and 25 keV, respectively, during the time of the radar-satellite experiment on December 8, 1971. Representative statistical counting errors are indicated.

The data for December 8 show a completely different character. During the period of interest, 1331:07 to 1331:11 UT, the measured flux varied by as much as an order of magnitude at the higher energies. In the absence of a corresponding variation in radar-observed electron densities, it seems probable that the satellite-observed variations are latitudinal rather than temporal. The consequences of such a latitudinal gradient will be discussed after the experimental results have been presented.

Figures 7 and 8 illustrate, for several times during each of the coordinated measurements, incident electron energy spectra obtained by the satellite instruments. The electron fluxes measured at the two angles differed by a factor of 2 or less over

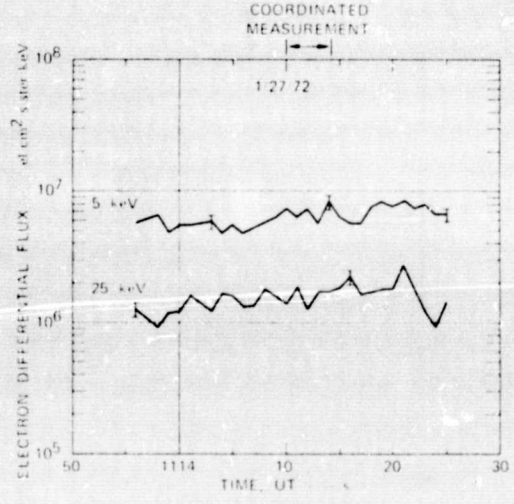

Fig. 6. Electron differential flux as a function of time for two satellite-mounted particle counters, centered at 5 and 25 keV, respectively, during the time of the radar-satellite experiment on January 27, 1972. Representative statistical counting errors are indicated.

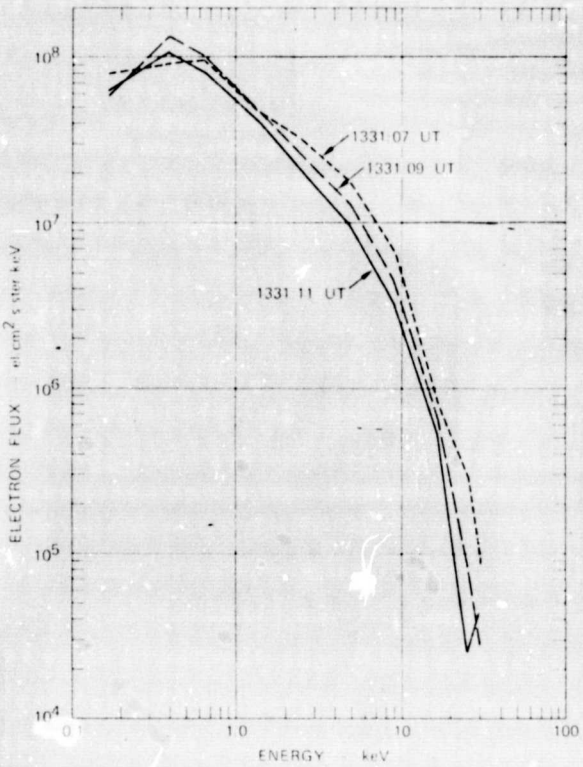

Fig. 7. Incident electron energy spectra determined from particle measurements on board the satellite 1971-089A during the coordinated radar-satellite experiment on December 8, 1971.

the energy range covered. The spectra shown in these figures were derived from an average of the fluxes measured at the two angles. The statistical counting errors were, in general, of the order of 20% or less. The 4-s integrations during each coordinated measurement are equivalent to averaging the three curves in each figure. It can be seen that the curves in Figure 7 are widely spread, especially at the higher energies, consistent with the gradient effects already discussed.

Experimental Results

Figure 3 (1331–1332 UT) and Figure 4 (1114–1115 UT) illustrate the radar-derived electron density data, and Figure 7 (1331:07 to 1331:11 UT, average) and Figure 8 (1114:10 to 1114:14 UT, average) illustrate the satellite-derived energetic electron flux data; these two types of data comprise the measurement inputs to the experiment. In order to provide information on electron production, the average electron flux spectra obtained from Figures 7 and 8 were assumed to be isotropically incident and were then used as input to the Lockheed Aurora computer program.

The Aurora program numerically solves the appropriate Fokker-Planck steady state diffusion equation to determine the electron flux spectrum along a geomagnetic field line associated with a given spectrum of incident auroral electrons. The solution takes into account atmospheric scattering, electron energy loss, and the mirroring effect of the geomagnetic field. The rate at which energy is deposited in the atmosphere by electrons is also calculated by the program. The theoretical solution of the diffusion equation was developed by *Walt et al.* [1968]. A detailed description of the computer program is given by *Cladis et al.* [1973].

The output of Aurora at each altitude is an estimate of the total electron energy deposited per cubic centimeter per second in the energy range above E_l, where E_l is an input to the program. The Aurora calculation has a lower-energy limit of 0.5 keV. Although it is true that 0.5-keV incident electrons do not penetrate the atmosphere to the altitudes considered, energy is nevertheless deposited at these altitudes in the energy range below 0.5 keV by higher-energy electrons scattering down in energy. Hence the calculated results must be extrapolated down to $E_l = 0$ in order to obtain an estimate of the total energy deposited at any particular altitude.

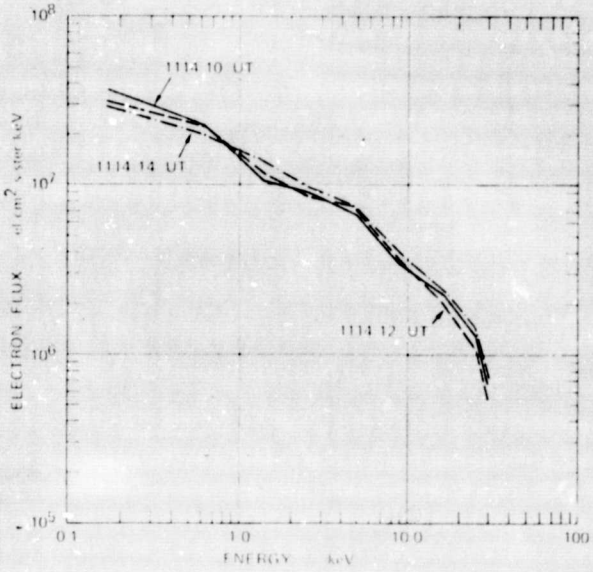

Fig. 8. Incident electron energy spectra determined from particle measurements on board the satellite 1971-089A during the coordinated radar-satellite experiment on January 27, 1972.

If we use the reasonable estimate of 35 eV of deposited electron energy corresponding, on the average, to the production of one electron-ion pair, the energy values provided by Aurora yield a direct estimate of the electron-ion production rate due to energetic electrons.

The Aurora calculation pertains only to production resulting from energetic electrons. A low intensity of energetic protons was observed to accompany the energetic electrons, and the total production taking place during auroral activity must include that due to energetic protons as well.

By using the method described by *Eather and Burrows*

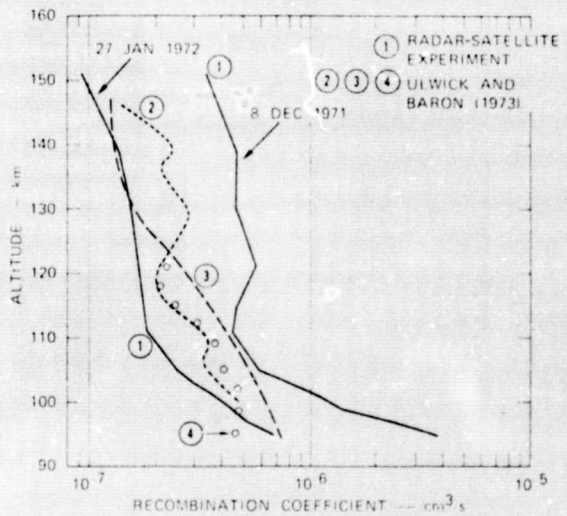

Fig. 9. Comparison of recombination coefficient profiles obtained from the radar-satellite experiment with profiles compiled by *Ulwick and Baron* [1973].

TABLE 1. Calculated Values of Electron-Caused Production, Proton-Caused Production, and Total Production at Various Altitudes

Altitude, km	December 8, 1971			January 27, 1972		
	Q_e	Q_p	Q_t	Q_e	Q_p	Q_t
151	2,660	10	2,670	1,155	250	1,405
139	4,560	13	4,573	2,193	380	2,573
130	7,450	21	7,471	3,875	640	4,515
121	11,250	28	11,280	7,305	930	8,235
115	13,850	34	13,880	11,150	1,120	12,270
111	15,050	37	15,090	14,900	1,250	16,150
105	13,450	13	13,460	20,460	800	21,260
103	11,680	10	11,690	22,200	480	22,680
101	9,350	8	9,360	23,400	160	23,560
99	6,140	6	6,150	23,100	0	23,100
97	4,030	3	4,030	21,500	0	21,500
95	2,780	0	2,780	17,250	0	17,250

Values are in electrons per cubic centimeter second.

[1966], electron-ion production profiles due solely to detected energetic protons were generated for the times 1331:07 to 1331:11 UT on December 8 and 1114:10 to 1114:14 UT on January 27, 1972. Total electron production was then taken to be the sum of the individual production rates due to energetic electrons and energetic protons. Table 1 lists values of electron-caused production Q_e, proton-caused production Q_p, and total production Q_t for each altitude at which the calculations were performed and for each of the coordinated measurements.

The overall uncertainties in Q_t are estimated to be less than 40%. These result from a combination of uncertainties in the absolute calibration of the sensors, counting statistics, deviations from isotropy, and calculational errors in the Aurora code. There are additional uncertainties resulting from spatial gradients in the particle fluxes. The latitudinal gradients in the observed fluxes are discussed later.

Applying the values of electron production from Table 1 and values of electron density from Figures 3 and 4 to (2) yields estimates of α.

The summarized results for both sets of coordinated measurements are given in Table 2 and are illustrated in Figure 9. It can be seen that the two α profiles varied with altitude in a similar manner but differed by a factor of about 3–4 over most of the altitude range, there being an increasing divergence below about 100 km.

DISCUSSION

It is instructive to compare the results in Table 2 with results for α obtained by other means. Figure 9 compares the present results (curves labeled 1) with results taken from *Ulwick and Baron* [1973]. Curve 2 is based on data taken directly from an instrumented rocket launched on March 16, 1972, into an aurora from the Poker Flat rocket range near Chatanika. Curve 2 illustrates the results of electron production determined from energetic particle measurements and electron density determined from plasma frequency measurements. Curve 3 illustrates the results of using (2) along with rocket-mounted mass spectrometer measurements of $n(NO^+)$ and $n(O_2^+)$ [*Sherman et al.*, 1973], laboratory values for $\alpha(NO^+)$ and $\alpha(O_2^+)$ [*Biondi*, 1969], and a Cira (1965) mean temperature model. Curve 4 illustrates results obtained on February 24, 1972, by applying the 'probability distribution' method to incoherent scatter measurement data [*Baron*, 1972]. It can be seen that the results of January 27, 1972, agree quite well with those results obtained by other means and that the α profile obtained on December 8, 1971, seems to be comparatively high at all altitudes.

Figure 10, taken directly from *Cladis et al.* [1973], presents a compilation of α values obtained during auroral activity by a number of workers. In the altitude range 100–125 km, α values given in Figure 10 vary over a range greater than 1 order of

TABLE 2. Calculated Values of Total Production, Electron Density, and Effective Recombination Coefficient at Various Altitudes for the Radar-Satellite Experiments

Altitude, km	December 8, 1971			January 27, 1972		
	Q_t, el/cm^3 s x 10^3	N, el/cm^3 x 10^5	α, cm^3/s x 10^{-7}	Q_t, el/cm^3 s x 10^3	N, el/cm^3 x 10^5	α, cm^3/s x 10^{-7}
151	2.67	0.88	3.45	1.405	1.23	0.93
139	4.57	0.98	4.76	2.573	1.38	1.35
130	7.47	1.27	4.63	4.515	1.71	1.42
121	11.28	1.50	5.69	8.235	2.21	1.68
115	13.88	1.72	4.69	12.27	2.65	1.75
111	15.09	1.83	4.50	16.15	2.96	1.84
105	13.46	1.51	5.90	21.26	2.92	2.50
103	11.69	1.21	8.00	22.68	2.75	3.00
101	9.36	0.91	11.30	23.56	2.54	3.65
99	6.15	0.66	14.1	23.1	2.28	4.45
97	4.03	0.41	24.0	21.5	2.02	5.28
95	2.78	0.27	38.1	17.25	1.60	6.74

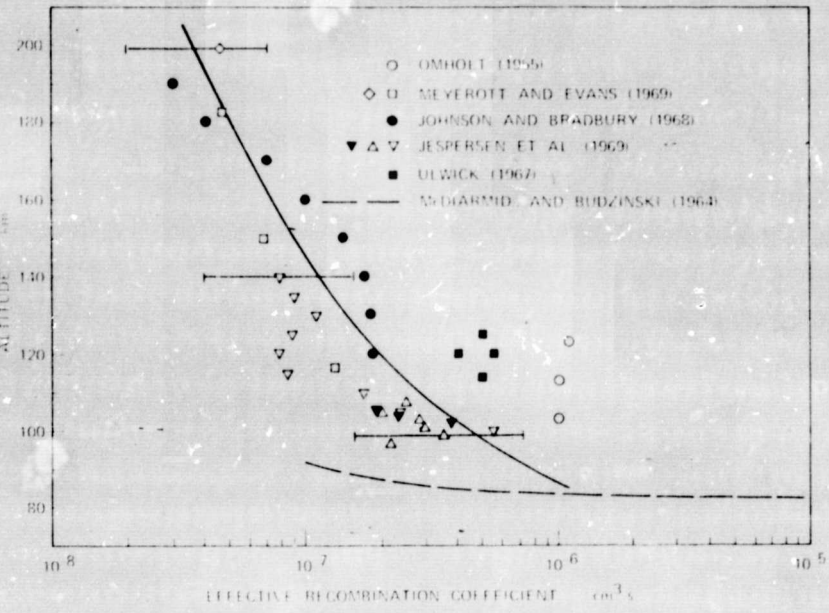

Fig. 10. Experimental values of the effective recombination coefficient α as a function of altitude [*Cladis et al.*, 1973]. The solid line represents a reasonable fit to the various data.

magnitude. The coordinated measurement results obtained here fall well within such an observed range of variation.

Although as just shown the results obtained here fall within the spectrum of results obtained by many others, there seems little reason to doubt that our results have been affected somewhat by spatial gradients over the measurement region.

From the discussion in the section on the experiment it is apparent that for the two coordinated measurements considered, the region over which the coordination took place extended about 20 km in longitude and about 30 km in latitude. We have no direct information on possible longitudinal gradients present during either measurement. During the January 27 measurement there seemed to be no significant latitudinal gradient present, and the January 27 results agreed quite well with results obtained elsewhere. During the December 8 measurement there was a significant latitudinal gradient, and the December 8 results agreed less well with other results. Regardless of the level of agreement of the December 8 results, it seems that data averaged across such a significant gradient should be considered with caution.

As was discussed earlier, the measurements described herein were coordinated to the extent of time coincidence but were not coordinated to the extent of providing intersection between the radar beam and the mapped trajectory of the satellite. Coordination to the extent of both spatial and temporal coincidence has been demonstrated at Chatanika and can easily be arranged in future experiments.

There is little doubt that a considerable reduction in integration time to the order of 1 s total can be effected with regard to measurements of energetic electron flux. By achieving spatial as well as temporal coincidence and reducing the integration time for measuring energetic electron flux to 1 s, the coordination region could be reduced to a horizontal dimension of about 10 km over much of the altitude range of interest.

Conclusions

The results obtained in this experiment demonstrate a very powerful technique for obtaining altitude profiles of the effective recombination coefficient in the auroral ionosphere. The results reported here were obtained from early measurements made by the Chatanika radar and the 1971-089A satellite.

The power and usefulness of the technique stem from the fact that a large number of reasonably accurate profiles of the recombination coefficient can be obtained during any day or other period of interest simply by making a coordinated measurement every time the orbiting satellite passes sufficiently near the radar location (typically 4 times each 24 hours). Each actual measurement (including logistics of coordination and data acquisition) is a fairly simple operation, especially in comparison with the complexity of an instrumented rocket shot.

The measurements described herein were not fully coordinated, and the consequent spatial separation of the radar and satellite measurements permitted the results to be influenced by horizontal gradients in electron density.

Fully coordinated measurements have been demonstrated, and the technique can be exploited in the future; the careful coordination of future measurements should greatly diminish the effects of horizontal gradients.

Acknowledgments. Discussions with J. B. Cladis and R. D. Sharp were very valuable. Barbara J. Giubbini provided a large portion of the data reduction. The satellite data were acquired and made accessible under the Office of Naval Research contract N00014-70-C-0203. This research was supported in part by the Defense Nuclear Agency under contracts DNA001-72-C-0076 (Stanford Research Institute) and DNA001-72-C-0178 (Lockheed) and in part by NASA under contract NASw 2582.

* * *

The Editor thanks I. G. Smith and E. V. Thrane for their assistance in evaluating this paper.

References

Baron, M. J., DNA project 617 radar: Auroral ionospheric measurements, final report, SRI project 1703, 297 pp., Stanford Res. Inst., Menlo Park, Calif., 1972.

Biondi, M. A., Atmospheric electron-ion and ion-ion recombination processes, *Can. J. Chem.*, *47*, 1710, 1969.

Cain, J. C., S. J. Hendricks, R. A. Langel, and W. V. Hudson, A proposed model for the international geomagnetic reference field—1965, *J. Geomagn. Geoelec.*, *19*, 335–355, 1967.

Cladis, J. B., G. T. Davidson, W. E. Francis, L. L. Newkirk, and M. Walt, Ionospheric disturbances affecting radio wave propagation, *LMSC/D315887, DNA 3103F*, 86 pp., Lockheed Palo Alto Res. Lab., Palo Alto, Calif., Aug. 1973.

Eather, R. H., and K. M. Burrows, Excitation and ionization by auroral protons, *Aust. J. Phys., 19*, 309, 1966.

Jespersen, N., B. Landmark, and K. Maseide, Comparison of auroral light emission and electron density, *J. Atmos. Terr. Phys., 31*, 1251, 1969.

Johnson, R. G., and J. N. Bradbury, Coordinated satellite and ionosonde measurements during auroral proton events (abstract), *Eos Trans. AGU, 49*, 735, 1968.

Leadabrand, R. L., M. J. Baron, J. Petriceks, and H. F. Bates, Chatanika, Alaska, auroral zone incoherent scatter facility, *Radio Sci., 7*, 747, 1972.

McDiarmid, I. B., and E. E. Budzinski, Angular distributions and energy spectra of electrons associated with auroral events, *Can. J. Phys., 42*, 2048, 1964.

Meyerott, R. E., and J. E. Evans, Coordinated measurements of particles, luminosity and electron concentrations, in *Atmospheric Emissions*, edited by B. M. McCormac and A. Omholt, p. 119, Van Nostrand Reinhold, New York, 1969.

Omholt, A., The auroral *E* layer and the auroral luminosity, *J. Atmos. Terr. Phys., 7*, 73, 1955.

Paschmann, G., E. G. Shelley, C. R. Chappell, R. D. Sharp, and L. F. Smith, Absolute efficiency measurements for channel electron multipliers utilizing a unique electron source, *Rev. Sci. Instrum., 41*, 1706, 1970.

Poppoff, I. G., and R. C. Whitten, DASA Reaction Rate Handbook, *DASA 1948*, pp. 8-1–8-17, Gen. Elec. Tempo, Santa Barbara, Calif., Sept. 1968.

Reed, R. D., E. G. Shelley, J. C. Bakke, T. C. Sanders, and J. D. McDaniel, A low-energy channel-multiplier spectrometer for ATS-E, *IEEE Trans. Nucl. Sci., NS-16*, 359, 1969.

Rishbeth, H., and O. K. Garriott, *Introduction to Ionospheric Physics*, 331 pp., Academic, New York, 1969.

Shea, M. F., G. B. Shook, J. B. Reagan, L. F. Smith, and T. C. Sanders, Channel multiplier instrumentation for the measurement of low energy auroral particles, *IEEE Trans. Nucl. Sci., NS-14*, 96, 1967.

Sherman, C., W. Swider, and R. S. Narcisi, Auroral ion composition measurements and model (abstract), *Eos Trans. AGU, 54*, 388, 1973.

Ulwick, J. C., Rocket measurements of auroral parameters, in *Aurora and Airglow*, edited by B. M. McCormac, p. 225, Reinhold, New York, 1967.

Ulwick, J. C., and M. J. Baron, Simultaneous rocket-probe and incoherent-scatter measurements during an aurora, paper presented at Incoherent Scatter Meeting, Union Radio Sci. Int., Tromsø, Norway, June 9–16, 1973.

Walt, M., W. M. MacDonald, and W. E. Francis, Penetration of auroral electrons into the atmosphere, in *Physics of the Magnetosphere*, edited by R. L. Carovillano and J. F. McClay, p. 534, Reinhold, New York, 1968.

Watt, T. M., Incoherent scatter observations of the ionosphere over Chatanika, Alaska, *J. Geophys. Res., 78*, 2992, 1973.

(Received May 15, 1974;
accepted August 7, 1974.)

Section 3
CHATANIKA/1971-89A CORRELATIONS

by P. M. Banks and E. G. Shelley

The Lockheed instrumentation aboard the 1971-89A spacecraft provides charged-particle measurements in a variety of energy channels adequate to determine the location of the auroral oval. Using these data, along with measurements of electric fields and currents from the Chatanika, Alaska incoherent scatter radar, a preliminary study has been undertaken to search for possible correlations in the two data sets. Particular emphasis was given to changes in the observed electric field which, on the basis of other studies, are known to depend upon substorms and/or changes in the size of the auroral oval.

The comparison day chosen for this study was 11 February 1972 corresponding to a 24-hour electric field experiment conducted at Chatanika. The observed variations of the ionospheric electric field, ionospheric height-integrated Hall and Pedersen conductivities and height-integrated electric current density are shown in Figures 3.1 and 3.2. During the period 04 UT (11 February) to 04 UT (12 February) five separate substorms occurred, as described previously by Banks et al. (1973). However, this particular day was not unduly disturbed in a global sense and the enhancements in conductivity and electric field are consistent with rather normal conditions when Chatanika rotates into a mildly expanded ($Q = 4$) auroral oval. Local K and K_p indices for College, given in Table 3.1, confirm the low level of the AE index (upper and lower) was about 200γ centered in the period 09 to 14 UT (11 February).

Specific substorms have been deduced from global magnetograms and the Chatanika data. These are given below for reference.

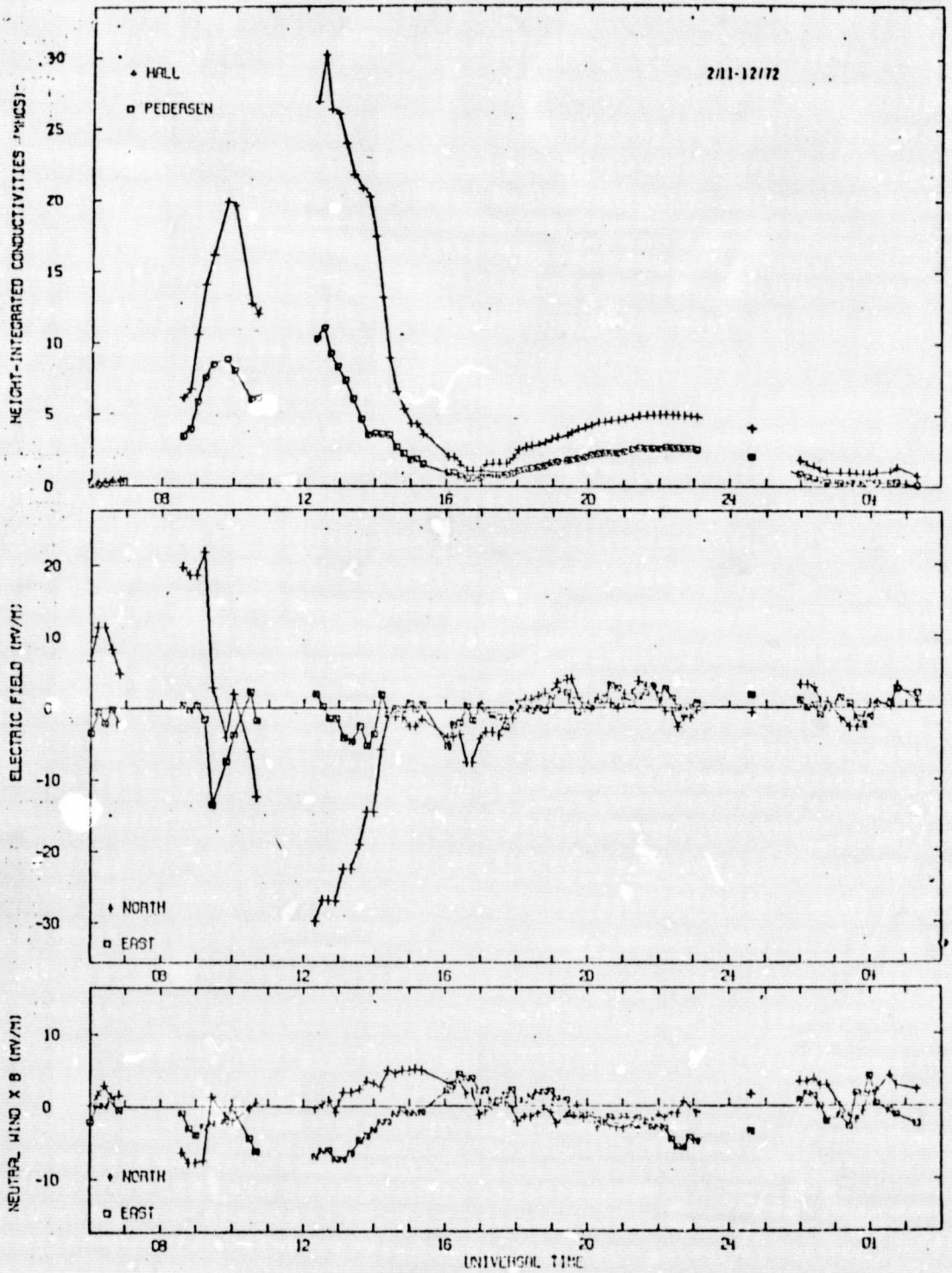

Figure 3.1. Measured values of height-integrated conductivities, electric field and E-region neutral winds for 11-12 February 1972 at Chatanika, Alaska.

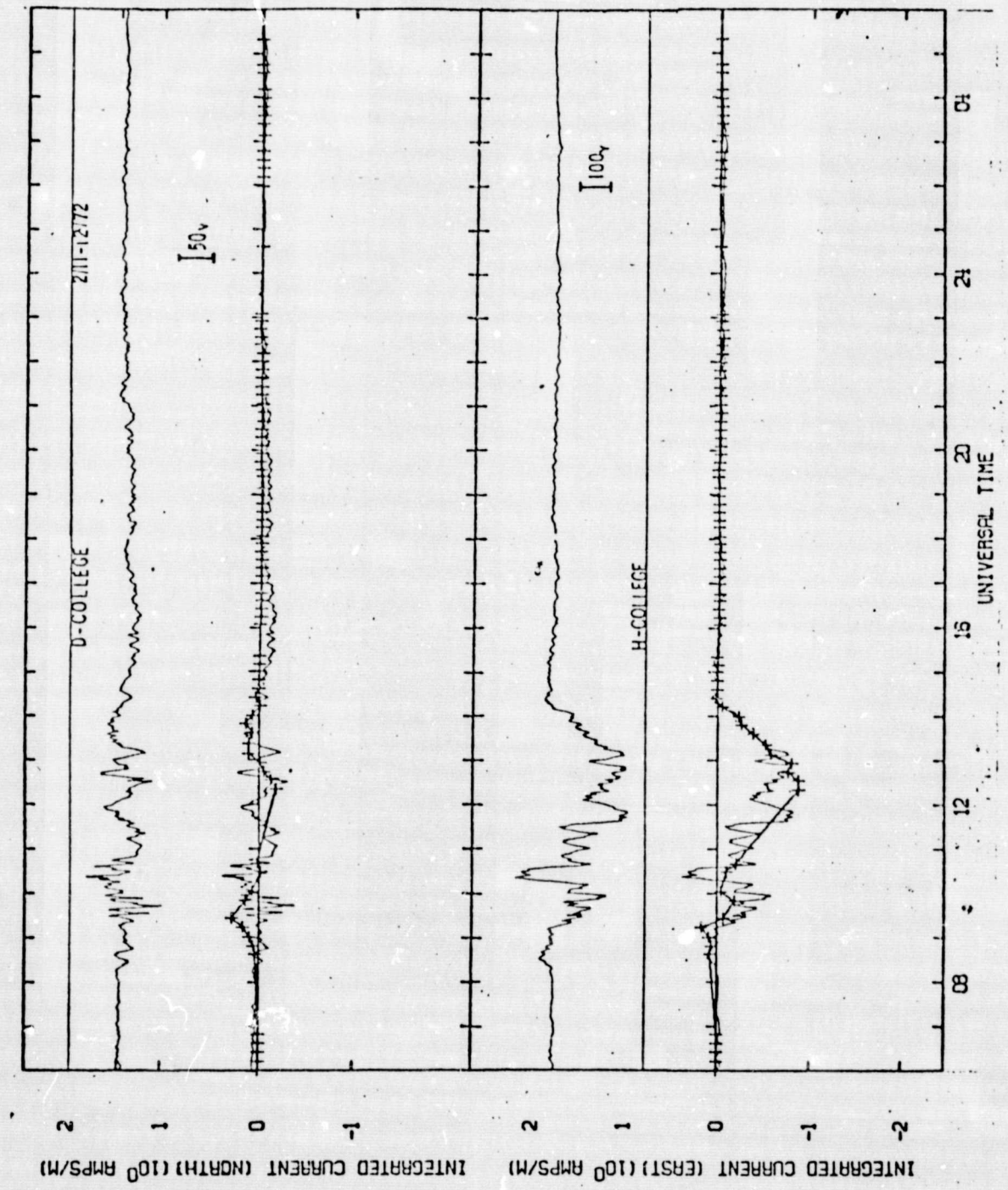

Figure 3.2. Measured height-integrated currents and observed magnetometer variation at Chatanika, Alaska for 11-12 February 1972.

Table 3.1

GEOMAGNETIC INDICES, 11-12 FEBRUARY 1972

Time (UT)	00	03	06	09	12	15	18	21	00	03	06
K (College)	2	1	0	2	5	4	1	0	0	0	0
K_p	3_o	2_o	1_o	2_+	3_o	2_o	1_+	1_-	1_+	2_+	2_+

0612 UT: A small enhancement in the northward electric field was seen at Chatanika with no corresponding increase in E-region conductivity or current density. Thus, this substorm was undetected by the Chatanika magnetometer.

0800 UT: The second substorm occurred two hours before local midnight with a possible increase in particle precipitation and simultaneous enhancement in electric field (a data gap occurs at substorm onset). Since the electric field was northward, a positive bay was registered by the Chatanika magnetometer.

0912 UT: The third substorm initiated the usual transition from north to south electric field found at the Harang discontinuity. Extensive particle precipitation took place and a 250γ negative bay resulted.

1610 UT: At this time Chatanika was in the morning sector. The substorm, seen in midnight sector magnetograms, resulted in a slight strengthening of the southward electric field.

0205 UT (12 February): A small electric field change was observed without particle precipitation, presumably because Chatanika was well south of the auroral oval at this time.

From an extensive analysis of Chatanika electric field data (see Banks and Doupnik, 1975) it is known that the intensity of the electric field measured at Chatanika is closely related to the proximity of the auroral oval. To a large extent, it appears that the global pattern of the electric field is strongly controlled by the oval. Thus, as the oval expands toward a fixed observing point such as Chatanika, one finds a rapid increase in $\underset{\sim}{E}_\perp$ while an oval contraction has the opposite effect. Even within the oval, as evidenced by particle precipitation, $\underset{\sim}{E}_\perp$ appears to grow as the poleward (or inner boundary) of the oval comes nearer.

In the normal course of events, Chatanika has a motion relative to the oval determined by the offsets of the geographic and geomagnetic axes. An electric field and conductivity pattern such as shown by Figure 3.1 is consistent with an initial approach, engulfment, and departure from the oval. In a specific way, then, the auroral oval establishes a natural coordinate system for studying electric fields. However, quantitative analyses based upon this idea have not yet been possible, primarily because it is very difficult

to establish from ground observations the precise location of the oval. Spacecraft measurements, of course, overcome part of this difficulty since they can provide specific locations for the portion of the oval intersected by the orbital trajectory. Such observations do not solve the general problem of oval location, however, for regions away from the spacecraft.

A possible solution to the problem of fixing the location of the auroral oval can be found by using the auroral oval observations reported by Feldstein and Starkov (1967). Taking measured intercepts of the auroral oval at a given geomagnetic local time and latitude, it is possible to search for an appropriate oval parameterized in terms of Q to deduce the global extent of the entire oval. By keeping track of northern and southern hemisphere auroral intercepts, the global extent of the oval can be monitored in a way not possible except through direct auroral imagery.

In the present study an initial attempt has been made to deduce the auroral oval location using boundary crossings taken from 1971-89A data. A summary of the data is given in Table 3.2 giving oval boundaries as defined through abrupt increases in the counting rate of the CME1D instrument which responds to electrons in the 0.98-1.82 keV energy range.

To show the connection between the observed auroral oval boundaries and those of Feldstein and Starkov, Figure 3.3 shows a Q = 4 oval marked with the observed particle precipitation regions. The results indicate good agreement, enough so that the location of the oval at intermediate points can be predicted with some degree of confidence. Unfortunately, the present data set had only two northern hemisphere passes which traversed the nightside oval. A similar study could be done with southern hemisphere passes if it were certain that the Feldstein ovals could be applied there.

In the present circumstances, there is no readily apparent change in the size of the auroral oval between 05 UT and 08 UT, i.e., the data fit the Q = 4 auroral oval. The Chatanika data indicate a first intersection with the oval

Table 3.2 .

AURORAL BOUNDARY OBSERVATIONS - 1971-39A DATA

11 February 1972

Code	Time (UT)	Latitude	Longitude	Comments
A	04:10:57	80.92°S	75.51°W	Entering quiet, non-dispersive nightside oval from equator.
B	05:00:35	79.94°N	95.34°E	Entering polar cusp from dayside. Gradual onset culminating in strong arc-like structures.
C	05:03:28	86.9°N	9.87°W	Exit polar cusp, enter polar cap.
D	05:14:01	52.84°N	70.48°W	Entering very narrow northern nightside auroral oval with well defined end point. Non-dispersive.
E	05:51:00	78.85°S	97.24°W	Entering very narrow southern nightside auroral oval with some dispersion of low-energy channels.
F	06:01:47	62.38°S	99.17°E	Continuation of pass with exit from polar cusp at indicated time. Cusp is greatly disturbed compared with northern hemisphere observation at 05:00:35 UT.
G	08:34:31	55.96°N	120.23°W	Passed through northern polar cap to nightside oval. Great dispersion of electron energies with latitude.
H	09:09:19	68.43°S	139.88°W	Continuation of previous pass to southern hemisphere midnight sector oval. Great dispersion of particles.
I	09:20:06	72.91°S	53.18°E	Polar cusp end of previous pass. Considerable structure in electron fluxes.

LOCKHEED PALO ALTO RESEARCH LABORATORY
LOCKHEED MISSILES & SPACE COMPANY, INC.
A SUBSIDIARY OF LOCKHEED AIRCRAFT CORPORATION

IMSC/D462625

at 0820 UT when the E-region electron density began to rise rapidly in response to substorm onset. According to Figure 3.3, rotation of the earth under a Q = 4 oval would result in Chatanika intercepting the oval at 0830 UT while for Q = 5 0800 UT is obtained. Thus, it appears that in the present case the increase in particle precipitation seen at Chatanika at 0820 UT was a result of relative motion between the observing site and a relatively stationary auroral oval. The substorm which took place at 0800 UT (based on all-sky camera data and global magnetograms) does not appear to have materially affected the oval itself.

Future studies based on this material should prove to be important to our knowledge of magnetospheric convection. The development of suitable auroral curves for the southern auroral zone is essential. However, once such curves are available, it should be possible to derive an extremely useful monitor of the average shape of the oval.

3.1 References

Banks, P. M., J. R. Doupnik, and S.-I. Akasofu, "Electric Field Observations by Incoherent Scatter Radar in the Auroral Zone," J. Geophys. Res., 78, 6607, 1973.

Feldstein, Y. I., and G. V. Starkov, "Dynamics of Auroral Belt and Polar Geomagnetic Disturbances," Planet. Space Sci., 15, 209, 1967.

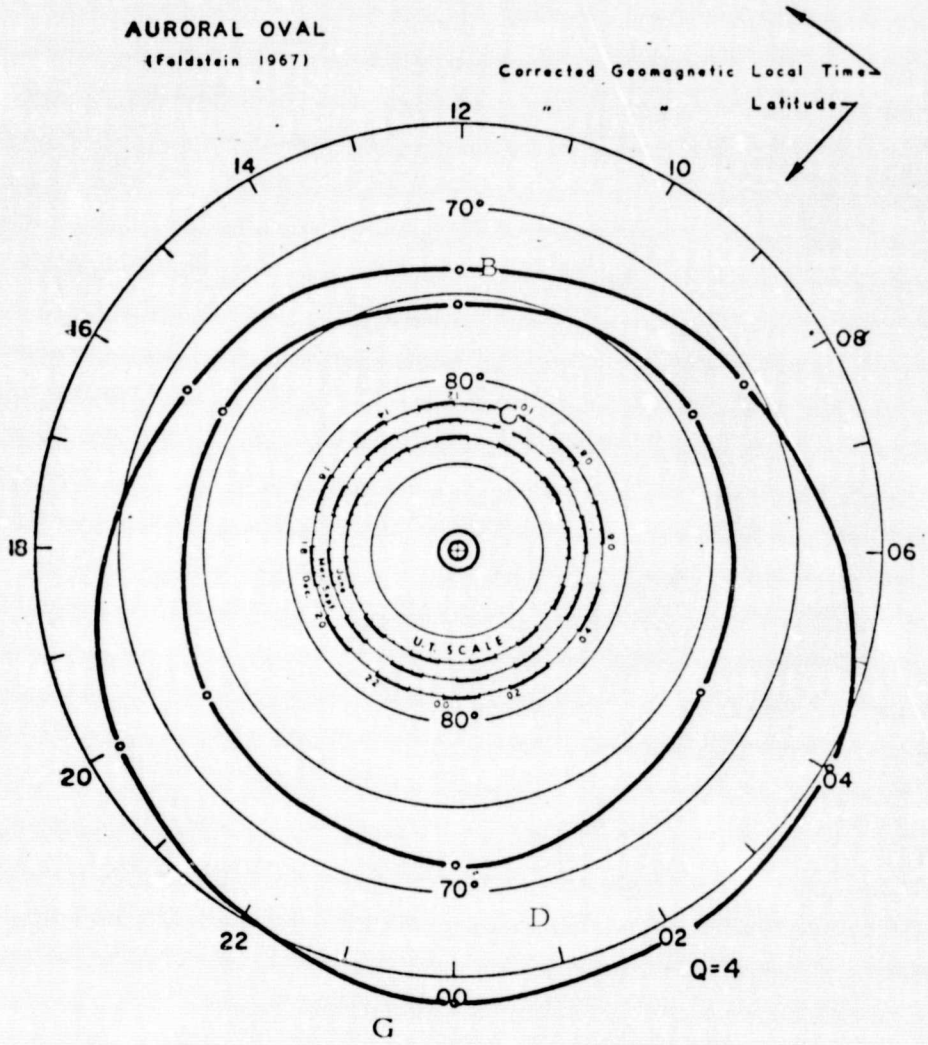

Figure 3.3. The Q = 4 Feldstein auroral oval is shown with four observed auroral oval boundaries deduced from 1971-89A data. Points B and D were obtained during a very quiet period while G followed a moderate substorm. Point C apparently is part of a sun-aligned auroral arc system.

Section 4

AURORAL BOUNDARY CHARACTERISTICS FROM 1971-89A PARTICLE DATA

by P. M. Banks and E. G. Shelley

The 1971-89A spacecraft orbit during February 1972 provides exceptionally good coverage of the polar cusp and the midnight sector auroral oval as seen through a variety of electron and proton detectors. In scanning a limited number of orbits a particular feature of the equatorward border of the auroral oval has become apparent. During magnetospherically quiet times the edges of the oval, as defined through various electron detectors in the enegyy range 0.16 to 8.8 keV, occur at the same point. For disturbed conditions following substorm activity, however, an energy dispersion is present such that the equatorward edge of the oval defined through, say, 0.16 keV electrons may be as much as 2^{o} of latitude lower than the onset measured at 4.7 keV.

Examples of this behavior are shown in Figures 4.1 and 4.2. In Figure 4.1 we show entry from mid-latitudes into a very narrow southern hemisphere midnight sector auroral oval characteristic of an undisturbed magnetosphere. The onset of the oval as seen in the 1.4, 2.6, 4.7, and 8.8 keV electron detectors is essentially the same. There is a slight tendency for the 0.16 and 0.6 keV electrons as well as 2.4 keV protons to rise slightly ($\sim$ 15 km) earlier. However, the difference is small compared with the data shown in Figure 4.2, taken at 0834 UT on a pass through the northern hemisphere polar cap and midnight sector oval. Here, electrons at 0.16 keV extend 185 km equatorward of the 8.8 keV electrons. A similar dispersion is seen in Figure 4.3 at 0909 UT upon entering the southern midnight sector oval.

The energy dispersion seen in Figures 4.2 and 4.3 corresponds to the hardening of the plasma sheet seen in spacecraft observations in the near magneto-

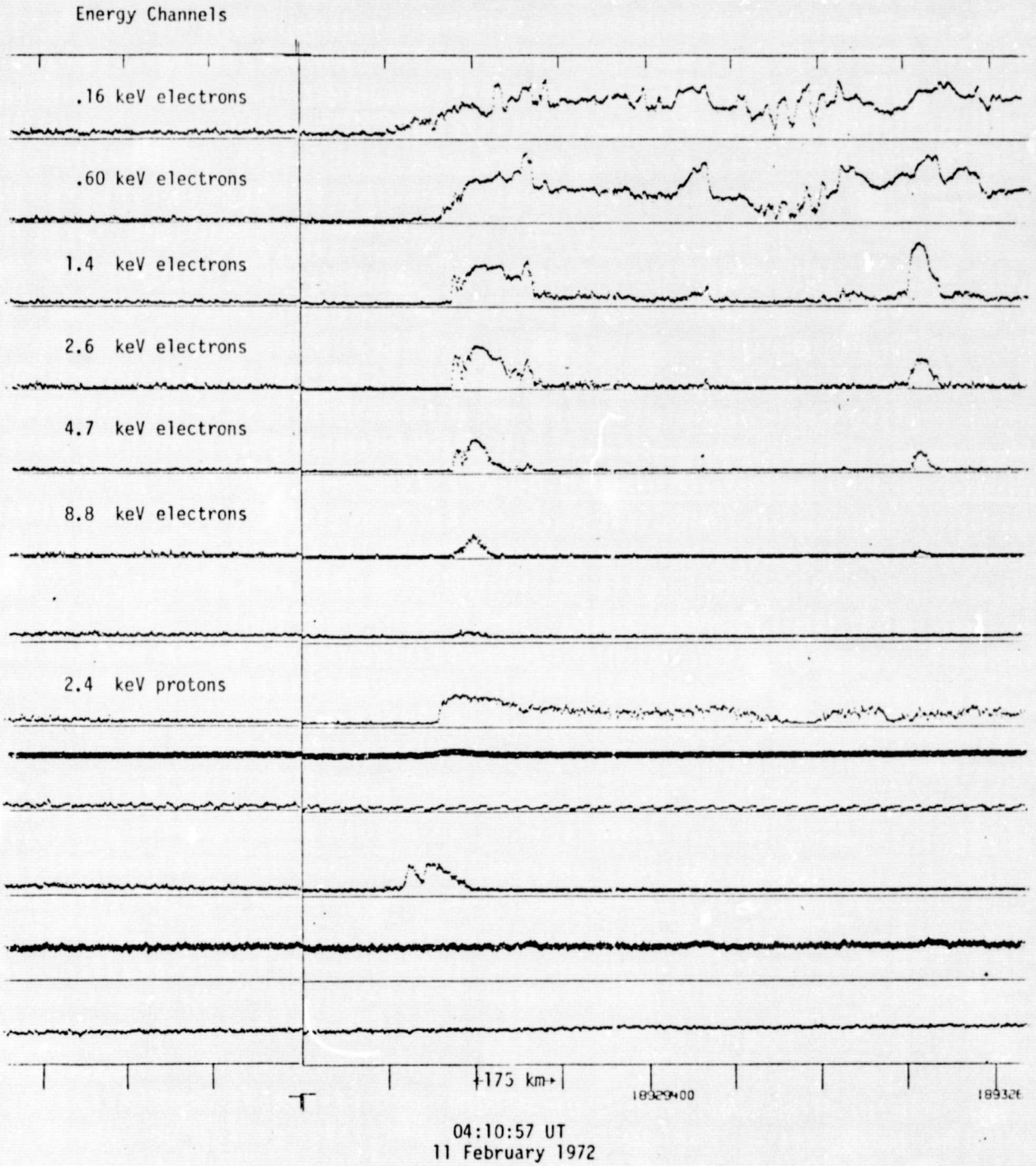

Figure 4.1. 1971-89A satellite particle data.

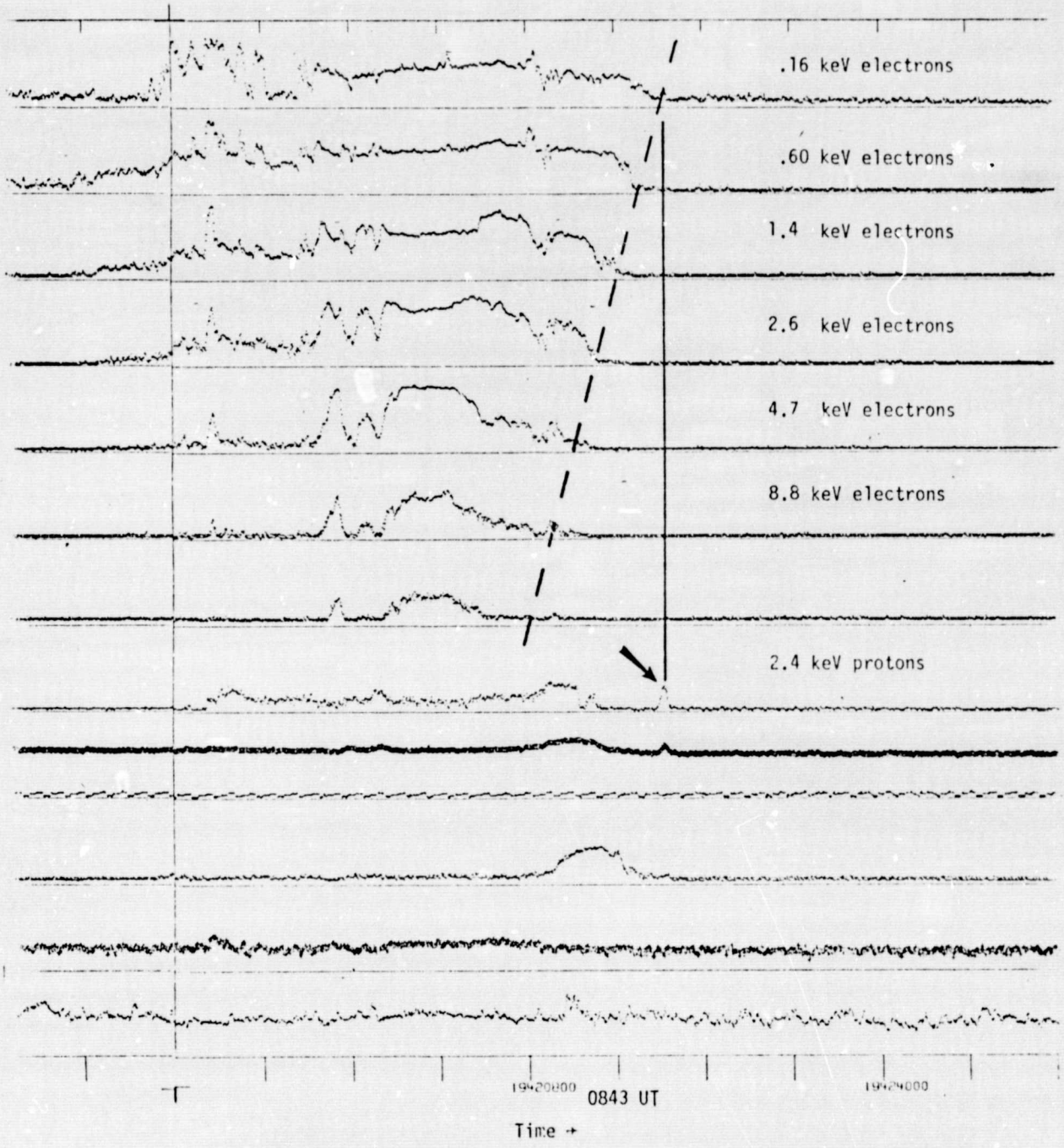

Figure 4.2. 1971-89A satellite particle data.

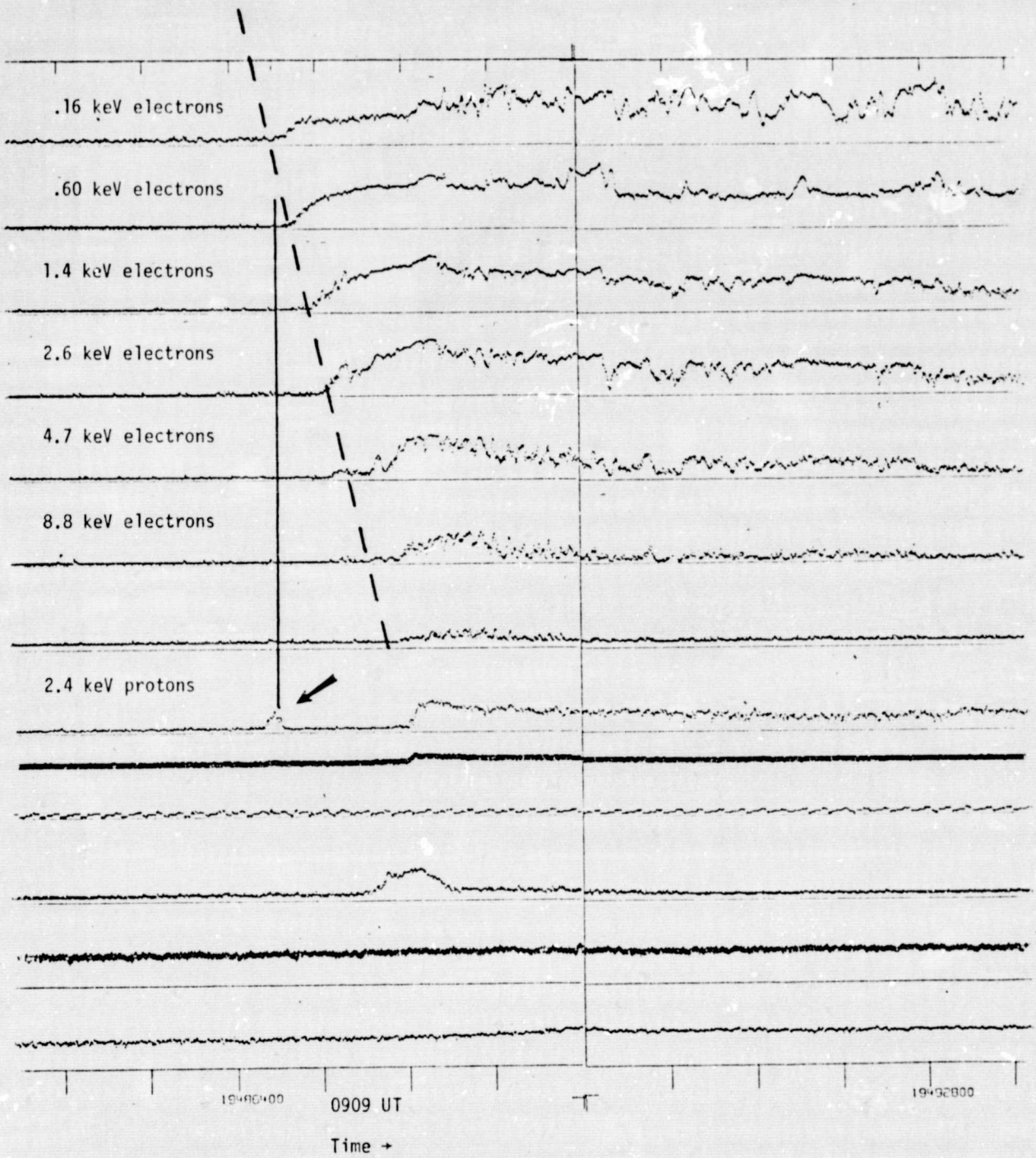

Figure 4.3. 1971-89A satellite particle data.

spheric tail. From the present results, it appears to be a feature of differential inward plasma motion of electrons acting under the influence of the cross-tail convection electric field, gradient drift and curvature drift effects. Low-energy electrons will move directly inward (to lower magnetic shells) while progressively higher-energy electrons will drift equatorward. Such an explanation only works, of course, if the source region of plasma sheet electrons is of limited spatial extent.

A separate, exciting feature of the present data is the appearance of a narrow spike of proton precipitation located equatorward of the main auroral oval precipitation. In Figure 4.2, for example, a spike of approximately 20 km width is seen 175 km equatorward of the high-energy particle oval. Interestingly, the spike occurs almost simultaneously with the onset of 0.16 keV electrons. This connection is also apparent in Figure 4.3.

If the spike of protons, seen in a small number of cases here, is a regular feature of disturbed times, it gives an interesting new clue to processes occurring at the plasma sheet boundary. Its possible connection with low-energy electron precipitation should be thoroughly studied.

Section 5

THE RELATIONSHIP OF AURORAL CURRENT SYSTEMS, PARTICLE PRECIPITATION, VISUAL AURORA, AND RADAR AURORA

by R. T. Tsunoda, T. Potemra, R. D. Sharp, E. G. Shelley, S.-I. Akasofu, and Y. Kamide

In this work we analyzed the auroral current system that existed during the local evening on 21 March 1973 by combining a number of different measurements. The data compiled for this tudy include those from the Homer 398 MHz phased-array radar, the Chatanika incoherent scatter radar, a NASA barium ion cloud, a meridian chain of magnetometers and all-sky camera stations, the APL magnetometer experiment on the TRIAD satellite, and the Lockheed auroral particle experiment on satellite 1972-76B. From this set of measurements we constructed a current system model that includes auroral electrojets, the Birkeland currents, and the associated charge carriers.

In summary, the preliminary results of the study are: (1) The eastward electrojet is driven by a poleward directed electric field and coincides with the zone of net downward Birkeland currents; (2) the net upward Birkeland currents occur in a region just poleward of the eastward electrojet but in a region also containing a poleward directed electric field; and (3) the closing current between the upward and downward Birkeland currents appears to be carried by a Pedersen current.

The poleward boundary of the eastward electrojet was found to approximately coincide with the trapping boundary for energetic ($E > 160$ keV) electrons. Part of the upward Birkeland currents are found to be carried by the precipitating auroral electrons and part of the downward Birkeland currents are found to be carried by the precipitating protons. A visual arc located on the poleward boundary of the eastward electrojet was found to be related to an "inverted V" precipitation event.

The Lockheed auroral particle experiment utilized in this work was part of a DARPA-funded program and was carried by the low-altitude polar-orbiting satellite 1972-76B. The satellite was launched on 2 October 1972 into a sun-synchronous noon-midnight orbit (inclination = 98.4°) with a perigee of 736 km and an apogee of 761 km. The satellite is spin stabilized with a period of approximately five seconds. The spin axis is perpendicular to the satellite orbital plane.

The auroral particle spectrometer consists of ten individual channels, each of which utilizes a channel electron multiplier as a sensor and a magnetic and/or foil threshold analysis to define the energy range of the selected particles. Table 5.1 lists the energy ranges of the individual channels. The spectrometer is oriented at 52.5° to the satelite spin axis such that it was sampling particles with pitch angles in the range from about 30° to 135° during the periods of interest (a pitch angle of 180° corresponds to particles coming down the field line). In addition to the auroral particle experiment, two channels from the more energetic particle spectrometers will be utilized. A plastic scintillation electron spectrometer (EEM) measured the integral electron fluxes with E > 160 keV and a solid-state proton spectrometer (LEP) measured the proton fluxes in the energy range from 120 to 250 keV. These two spectrometers were oriented at 90° to the satellite spin axis providing measurements of both the precipitating and trapped energetic particle fluxes.

The satellite data on the two passes of interest on 21 March 1973 are shown in Figures 5.1 and 5.2. The peak precipitated count rate per spin as a function of universal time and satellite location is illustrated. The isotropy (I) and cutoff (C) trapping boundaries for E > 160 keV electrons defined by the EEM detector are indicated along the abscissa.

Figure 5.3 summarizes the auroral conditions during this period. The contours of constant ΔH, the disturbance in the horizontal component of the geomagnetic field, were constructed from magnetograms from Sitka, College, Fort Yukon, Inuvik and Mould Bay. The latitudinal extent of the radar aurora, as

Table 5.1

LOCKHEED PARTICLE DETECTORS

Detector Name	Particles Measured	Energy Range (keV)
CME-A	Electrons	0.07 - 0.21
CME-B	Electrons	0.20 - 0.59
CME-C	Electrons	0.50 - 1.5
CME-D	Electrons	1.5 - 4.5
CME-E	Electrons	4.6 - 13.7
CME-F	Electrons	13.6 - 40.7
CMP	Protons	0.7 - 2.1
CFP-A	Protons	> 13.0
CFP-C	Protons	> 41.0
CZU	Ultraviolet Background	------
EEM	Electrons	> 160
LEP	Protons	120 - 250

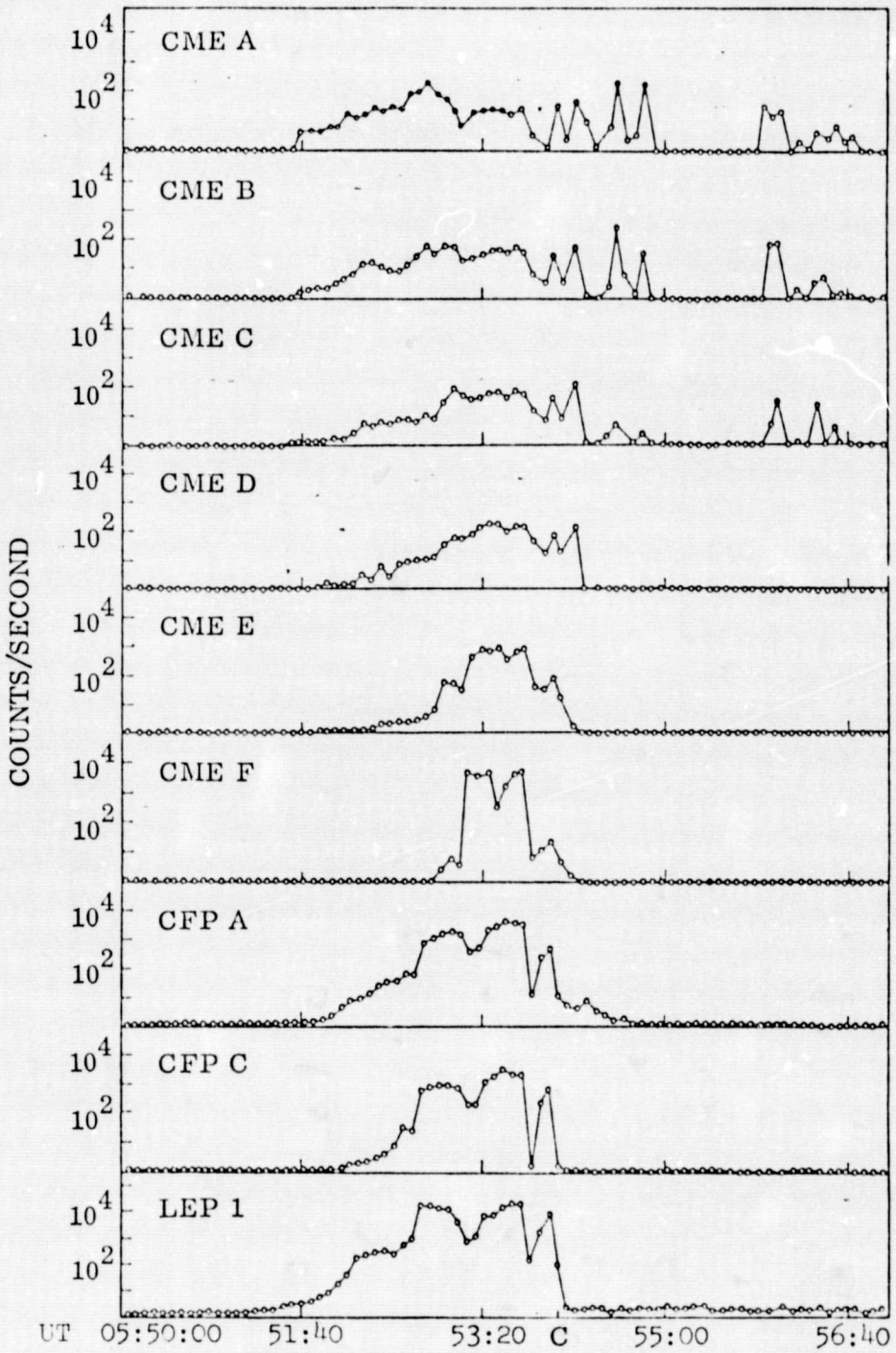

Figure 5.1. Satellite measurements of particle fluxes on 21 March 1973.

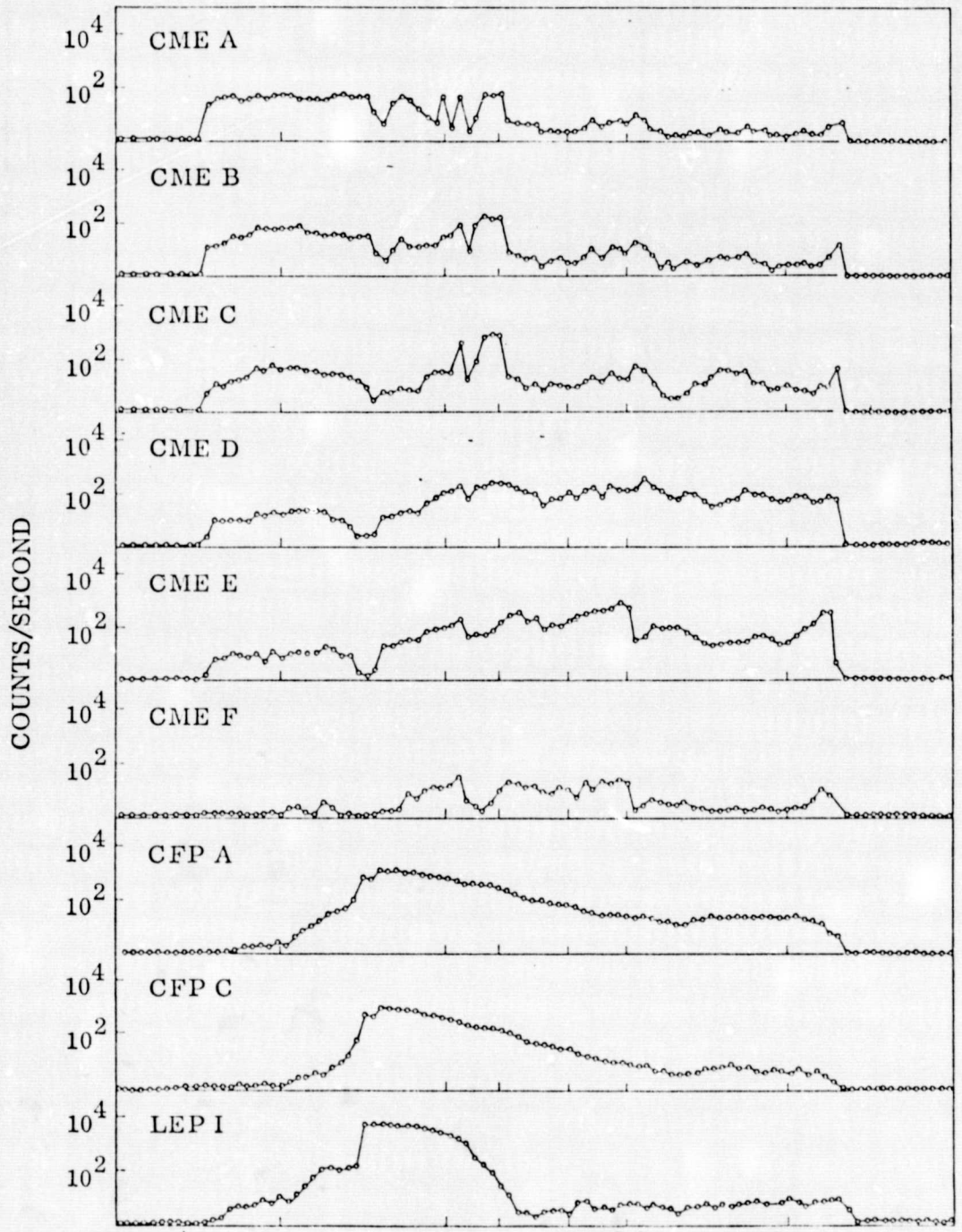

UT	07:31:40	33:20	35:00 I	C 36:40	38:20	40:00
N. LAT	46.6°	52.5°	58.3°	64.1°	69.6°	74.9°
W. LONG	123.2°	125.7°	128.8°	133.1°	139.4°	149.4°
λ_L	54.2°	59.2°	63.9°	68.2°	72.0°	74.9°

Figure 5.2. Satellite measurements of particles fluxes on 21 March 1973.

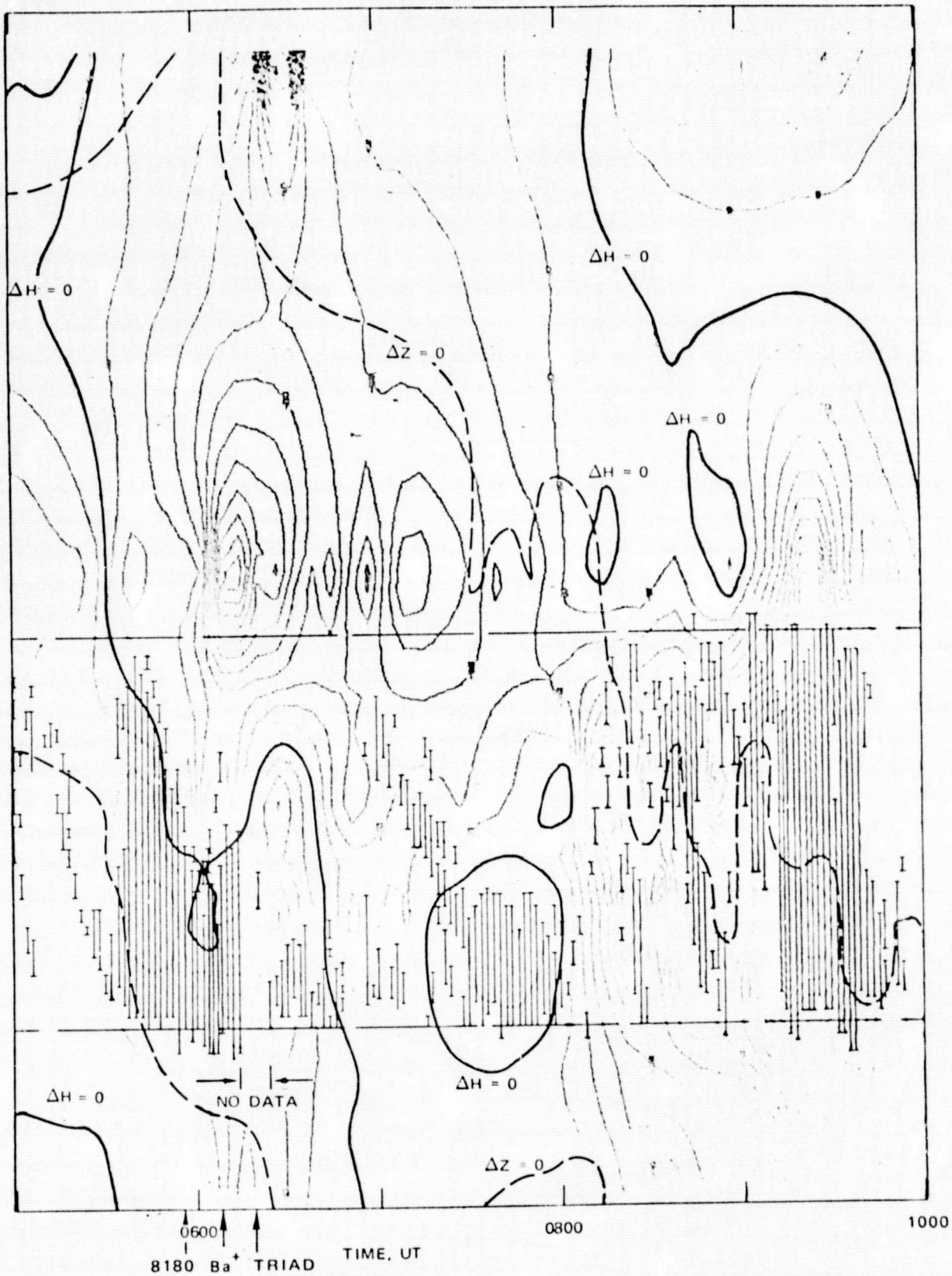

Figure 5.3. Contours of constant ΔH and latitudinal extent of radar aurora (vertical lines) on 21 March 1973.

observed by the 298-MHz phased array at Homer, is indicated by the vertical line segments superimposed over the constant ΔH contours. The two dashed horizontal lines are at latitudes of 63° and 69.5° and indicate the radar visibility boundaries. The geometry of the coordination on the second of the two satellite passes is illustrated in Figure 5.4. The grey scale indicates the intensity of the radar backscatter at the time of the satellite transit. A comparison of Figures 5.2 and 5.4 show that the trapping boundary coincides approximately to the magnetic latitutde of the poleward boundary of the radar echo.

The observed relationships on this night between the electric fields, electron densities, particle precipitations, radar returns, ionospheric electrojet currents, Birkeland currents, and optical aurora are quite complex and not yet completely understood. An initial paper emphasizing the phenomenological aspects of the coordinated data is currently being prepared for submission to the Journal of Geophysical Research.

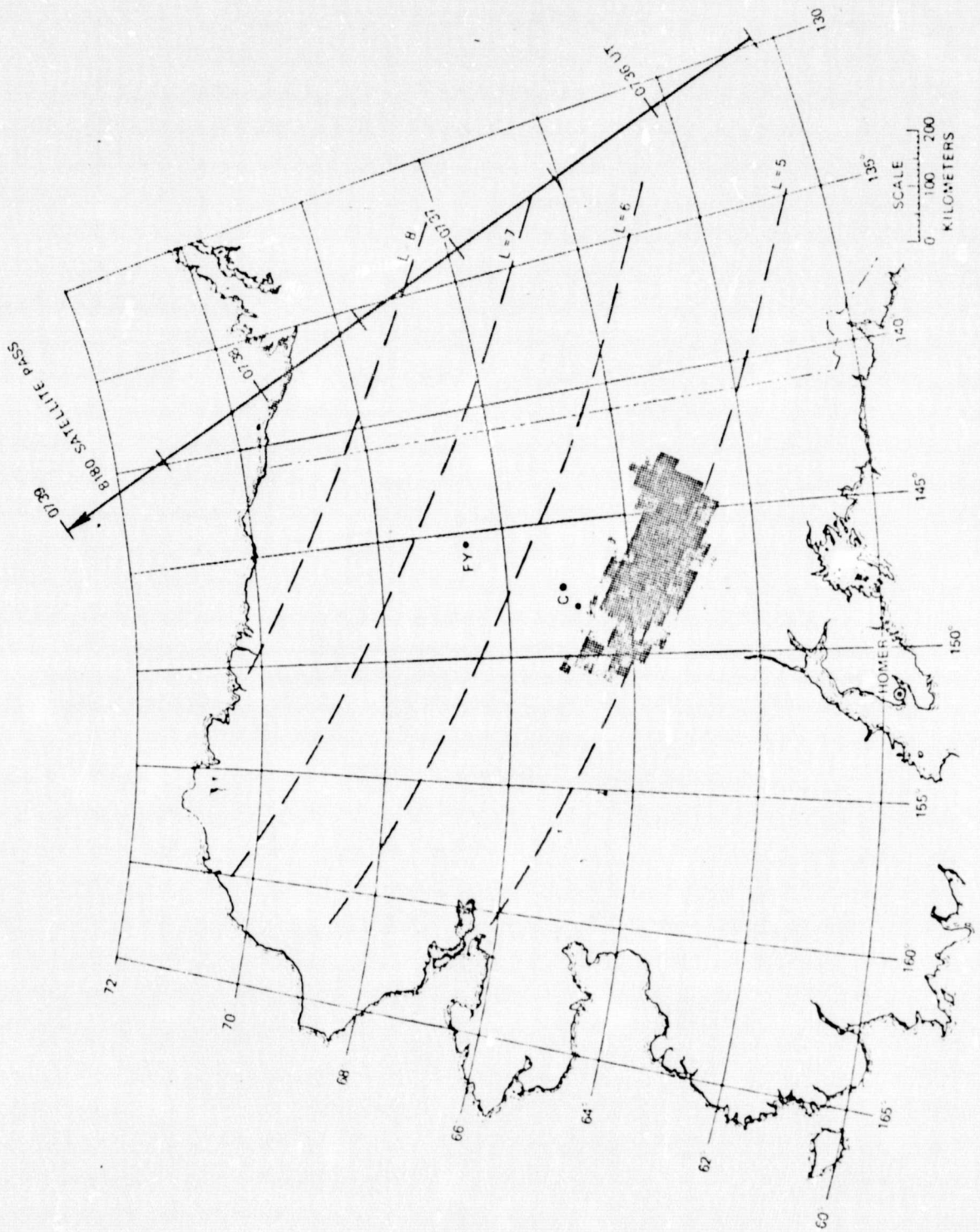

Figure 5.4. Coordination geometry on second satellite overpass on 21 March 1973.

VOL. 79, NO. 31 JOURNAL OF GEOPHYSICAL RESEARCH NOVEMBER 1, 1974
Page 4725

Section 2

Joint Radar-Satellite Determination of the Effective Recombination Coefficient in the Auroral *E* Region

T. M. WATT

Stanford Research Institute, Menlo Park, California 94025

L. L. NEWKIRK AND E. G. SHELLEY

Lockheed Palo Alto Research Laboratory, Palo Alto, California 94304

This paper reports on the experimental determination of the effective recombination coefficient α in the auroral *E* region. The technique consists of obtaining measurements, time coincident and nearly space coincident, of electron density from the Chatanika incoherent scatter radar and of electron production rate from the 1971-089A satellite. Electron density profiles are determined along the radar beam, and electron production profiles are field aligned. The horizontal separation caused by these and other factors can give rise to uncertainties in the presence of horizontal gradients in electron density or production. Values of α obtained by this technique are nevertheless in reasonable agreement with the results of others. Since the technique offers the possibility of frequent and routine determinations of α profiles (typically, four per day), it clearly represents a powerful means for providing synoptic studies of this ionospheric parameter.

At present there is a very high degree of interest in physical processes associated with the auroral ionosphere. In the *D* and *E* regions of the auroral ionosphere the parameter effective recombination coefficient α is of interest because of its relationship to electron-ion loss processes, and it is studied by a variety of techniques [*Biondi*, 1969; *Baron*, 1972; *Ulwick and Baron*, 1973].

The purpose of this paper is to present the results of a new technique to determine height profiles of α in the auroral *E* region. The technique combines height profiles of electron density from the Chatanika incoherent scatter radar [*Leadabrand et al.*, 1972] with coincident field-aligned profiles of electron production obtained from energetic particle measurements made by the 1971-089A satellite. Potentially, the power of this technique for synoptic studies of α is enormous in comparison with existing methods, since, in principle, a separate measurement can be made on every satellite pass occurring near the radar (typically, four per day).

In the *E* region the effects of negative ions can be neglected [*Biondi*, 1969]. If we also assume that plasma transport effects are negligible, then the steady state equation of continuity is given approximately by [*Rishbeth and Garriott*, 1969]

$$Q = \alpha N^2 = \{\alpha(NO^+)n(NO^+) + \alpha(O_2^+)n(O_2^+)\}N \quad (1)$$

from which it follows that

$$\alpha = Q/N^2 = [\alpha(NO^+)n(NO^+) + \alpha(O_2^+)n(O_2^+)]/N \quad (2)$$

where

Q electron production rate;
N electron number density;
$\alpha(X^+)$ recombination coefficient of ion species X^+;
$n(X^+)$ number density of ion species X^+;
α effective recombination coefficient.

In addition to its dependence on species and number density of ions, α is dependent on neutral density [*Poppoff and Whitten*, 1968] and is temperature sensitive [*Biondi*, 1969].

As is indicated in (2), α can be experimentally determined from the quotient Q/N^2. The efficacy of such a determination rests on obtaining time and space coincident measurements of electron production rate and electron number density.

At any instant of time the radar obtains a range profile of electron density along the antenna beam, and the satellite obtains an in situ measurement of the energy spectrum and pitch angle distribution of precipitating particles at the position of the satellite (~800-km altitude). The instantaneous measurement at the satellite can, by using an appropriate computer code, be transformed into an electron production profile along the geomagnetic field line [*Cain et al.*, 1967] passing through the satellite. The essence of the experiment is to coordinate the radar operation, both in time and in antenna pointing angle, to obtain an intersection between a radar-obtained density profile and a satellite-obtained production profile.

The best possible geometrical circumstance for a coordinated measurement would be that the satellite would pass through that geomagnetic field line occupied by the radar. The radar antenna beam could then be directed up the field line, and if the small amount of curvature in the field line is neglected, the production and density profiles would be congruent. Realistically, of course, this condition is never achieved, and in any actual measurement the field line profile of production and the antenna beam profile of density are skew with respect to each other and can intersect at only one place. When such skewness exists, a particular altitude must be chosen at which intersection is to take place.

INSTRUMENTATION

The Chatanika facility is an *L* band (1290 MHz) fully steerable incoherent scatter radar system located at 65.1°N, 147.45°W (L = 5.7) near Fairbanks, Alaska. The system has been described in considerable detail [*Leadabrand et al.*, 1972; *Baron*, 1972; *Watt*, 1973] and will not be described further here.

The 1971-089A satellite was in a nearly circular 93° inclination orbit at approximately 800 km. The satellite was three-axis stabilized and geocentrically oriented. The particle data utilized here were obtained from two sets of fixed energy detectors oriented at 15° and 55°, respectively, from the local zenith. The electron instruments consisted of 180° permanent

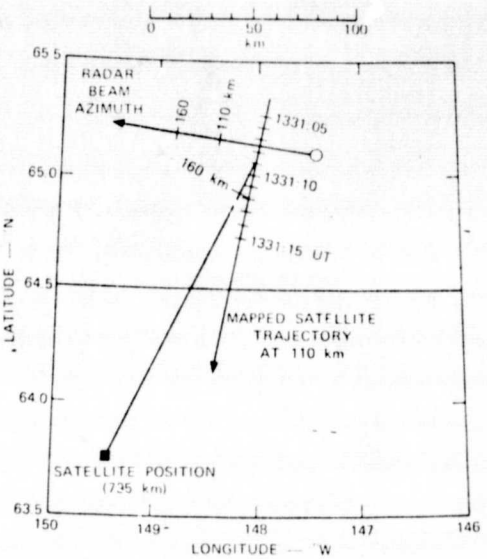

Fig. 1. Plan view geometry of the radar beam and the mapped trajectory of the satellite during the coordinated experiment on December 8, 1971.

magnet spectrometers with channeltron detectors. There were seven independent sensors at 15° and nine independent sensors at 55°. The instruments had contiguous energy passbands of $\Delta E/E$ between 0.60 and 1.10 and provided complete coverage of the electron fluxes from approximately 70 eV to 40 keV at both angles. The proton data used here were derived from integral flux detectors with proton thresholds at 16 and 39 keV at each of the two angles. These types of instruments have been described in more detail by *Shea et al.* [1967], *Reed et al.* [1969], and *Paschmann et al.* [1970].

The pulses from each sensor output were fed into a log count rate meter with a time constant of approximately 300 ms. The rate meters were sampled by the telemetry approximately 5 times per second. This analysis utilized one sample per second from each detector.

Experiment

During the period October 1971 through April 1972, several radar-satellite coordinated measurements were made, and these measurements comprise the data base for this study. At the time of these measurements, the radar was being operated according to other unrelated experiments, so that the radar antenna was not pointed so as to provide optimal coincidence with the satellite measurements.

From the total data base, two events, occurring at 1331 UT (0331 LST, 124° solar zenith angle) on December 8, 1971, and at 1114 UT (0114 LST, 132° solar zenith angle) on January 27, 1972, were selected for detailed analysis. The contrasting results of these two events demonstrate both the efficacy of the technique and certain limitations on quantitative conclusions.

The spatial criterion for the coordinated measurements is given by the requirement that at 110-km altitude, the radar beam and field-line-mapped position of the satellite lie on the same geomagnetic latitude. This coordination criterion is consistent with typical radar observations of auroral E ionization in which maximum electron densities occur near 100–120 km and latitudinal density gradients are much larger than longitudinal density gradients [*Baron*, 1972].

Figures 1 and 2 illustrate plan views of the two measurements plotted in geographic coordinates for December 8 and January 27, respectively. Each figure illustrates the mapped trajectory of the satellite at 110-km altitude, the projection of the radar beam and its location at 110-km altitude, and the point on the mapped trajectory corresponding to the geomagnetic latitude of the 110-km intersection of the radar beam.

It can be seen from the figures that, by our criterion, the optimal times for the coordinated measurements are 1331:09 UT on December 8 and 1114:12 UT on January 27 and the horizontal distances (at 110-km altitude) between the corresponding electron density and electron production measurements are about 21 and 18 km, respectively.

The measured data from both the radar and the satellite were integrated over finite times in order to reduce statistical fluctuations to acceptable levels. This requirement is illustrated for the radar measurements on December 8 and January 27 in Figures 3 and 4, respectively, which present for each case overlays of three electron density profiles obtained by the radar while the satellite was passing nearby. It can be seen that for these cases the electron density maximums occur near 110-km altitude. We can associate the large high-altitude fluctuations appearing in the 10-s or 20-s profiles with statistical noise fluctuations in the radar receiver; thus it is apparent that no large temporal variations in electron density are being observed during the 1-min periods on either December 8 or January 27. Accordingly, in order to provide valid electron density data relatively free from statistical noise effects, we take the 1-min electron density profiles as comprising the radar input to the coordinated measurements. In the altitude range below 150 km the standard deviation of statistical errors using a 1-min integration is estimated to be less than 8×10^3 el/cm^3.

As was pointed out in the previous section, a complete data set was obtained from the satellite instrumentation once per second. These particle data were then averaged over a period of 4 s, corresponding to a distance traveled along the mapped trajectory of about 28 km (see Figures 1 and 2).

Figures 5 and 6 illustrate the second-by-second outputs of two of the satellite-mounted electron sensors for time periods encompassing each of the two specific measurement times. The curves illustrate the differential electron flux in the energy

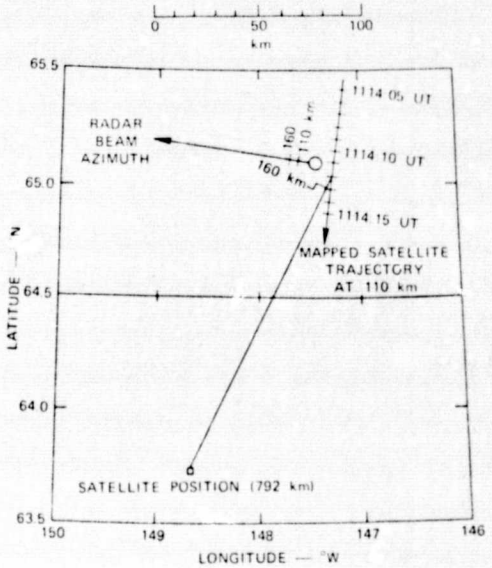

Fig. 2. Plan view geometry of the radar beam and the mapped trajectory of the satellite during the coordinated experiment on January 27, 1972.

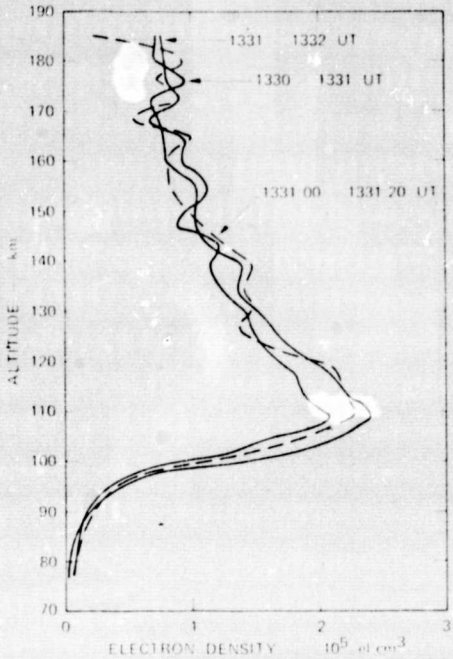

Fig. 3. Electron density profiles obtained from radar measurements during the coordinated radar-satellite experiment on December 8, 1971.

ranges indicated. These curves are representative of flux variations over the entire energy range measured. Representative statistical uncertainties associated with the measured values are indicated by the error bars.

The data for January 27 show a variation of much less than a factor of 2 over the 4-s period 1114:10 to 1114:14 UT. Aside from the small fluctuations present in the second-by-second data, the measured flux did not exhibit any significant latitudinal variation in the vicinity of Chatanika.

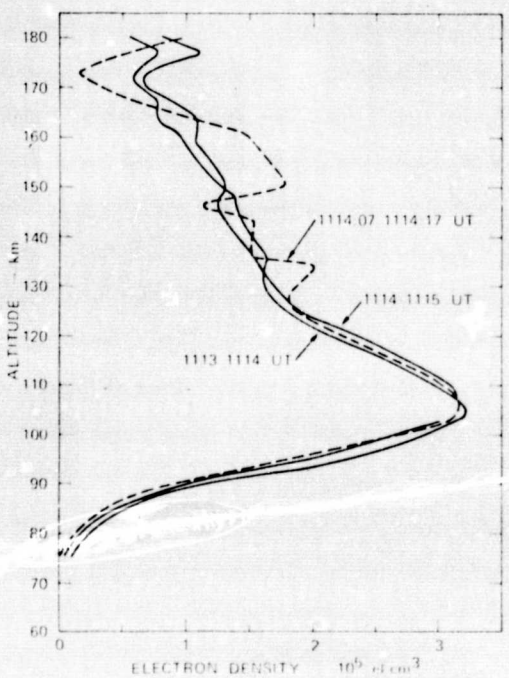

Fig. 4. Electron density profiles obtained from radar measurements during the coordinated radar-satellite experiment on January 27, 1972.

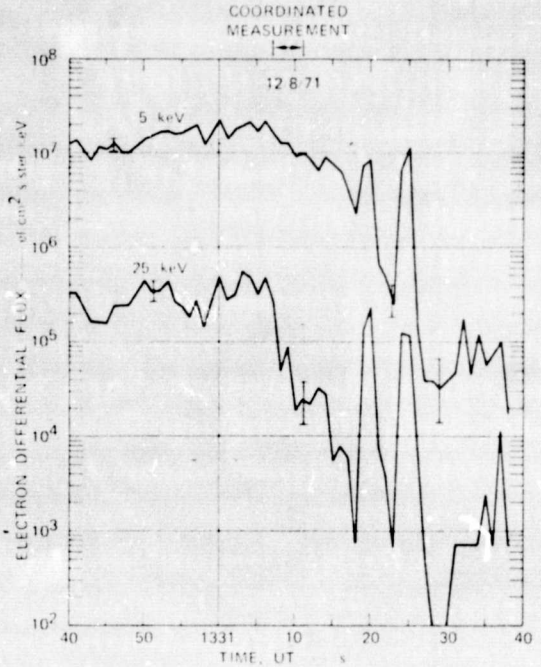

Fig. 5. Electron differential flux as a function of time for two satellite-mounted particle counters, centered at 5 and 25 keV, respectively, during the time of the radar-satellite experiment on December 8, 1971. Representative statistical counting errors are indicated.

The data for December 8 show a completely different character. During the period of interest, 1331:07 to 1331:11 UT, the measured flux varied by as much as an order of magnitude at the higher energies. In the absence of a corresponding variation in radar-observed electron densities, it seems probable that the satellite-observed variations are latitudinal rather than temporal. The consequences of such a latitudinal gradient will be discussed after the experimental results have been presented.

Figures 7 and 8 illustrate, for several times during each of the coordinated measurements, incident electron energy spectra obtained by the satellite instruments. The electron fluxes measured at the two angles differed by a factor of 2 or less over

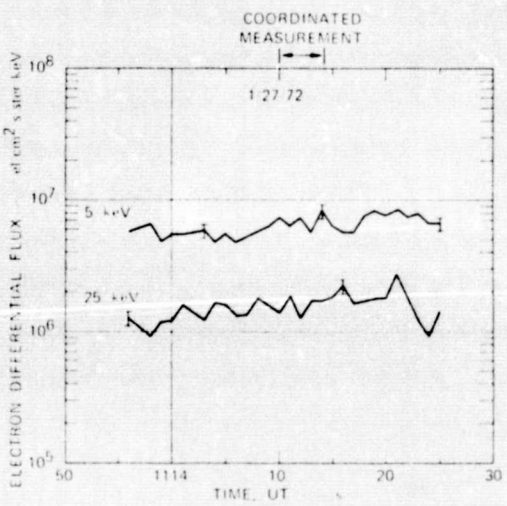

Fig. 6. Electron differential flux as a function of time for two satellite-mounted particle counters, centered at 5 and 25 keV, respectively, during the time of the radar-satellite experiment on January 27, 1972. Representative statistical counting errors are indicated.

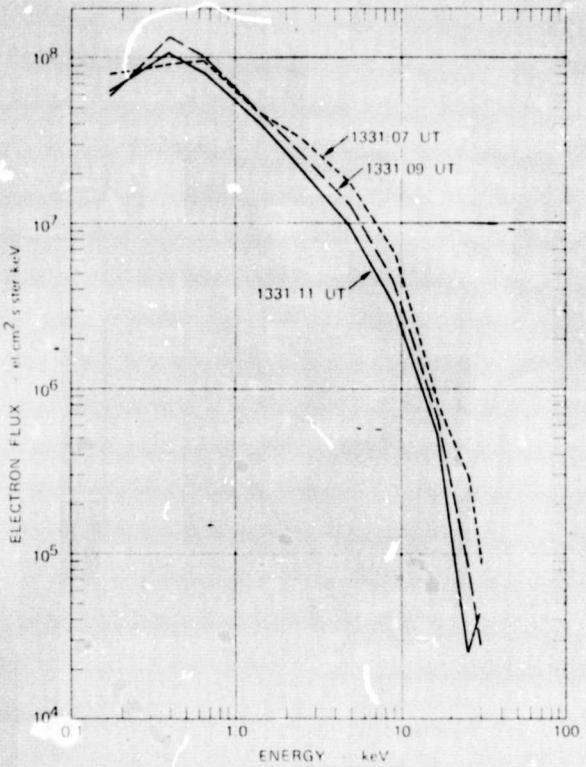

Fig. 7. Incident electron energy spectra determined from particle measurements on board the satellite 1971-089A during the coordinated radar-satellite experiment on December 8, 1971.

the energy range covered. The spectra shown in these figures were derived from an average of the fluxes measured at the two angles. The statistical counting errors were, in general, of the order of 20% or less. The 4-s integrations during each coordinated measurement are equivalent to averaging the three curves in each figure. It can be seen that the curves in Figure 7 are widely spread, especially at the higher energies, consistent with the gradient effects already discussed.

Experimental Results

Figure 3 (1331–1332 UT) and Figure 4 (1114–1115 UT) illustrate the radar-derived electron density data, and Figure 7 (1331:07 to 1331:11 UT, average) and Figure 8 (1114:10 to 1114:14 UT, average) illustrate the satellite-derived energetic electron flux data; these two types of data comprise the measurement inputs to the experiment. In order to provide information on electron production, the average electron flux spectra obtained from Figures 7 and 8 were assumed to be isotropically incident and were then used as input to the Lockheed Aurora computer program.

The Aurora program numerically solves the appropriate Fokker-Planck steady state diffusion equation to determine the electron flux spectrum along a geomagnetic field line associated with a given spectrum of incident auroral electrons. The solution takes into account atmospheric scattering, electron energy loss, and the mirroring effect of the geomagnetic field. The rate at which energy is deposited in the atmosphere by electrons is also calculated by the program. The theoretical solution of the diffusion equation was developed by *Walt et al.* [1968]. A detailed description of the computer program is given by *Cladis et al.* [1973].

The output of Aurora at each altitude is an estimate of the total electron energy deposited per cubic centimeter per second in the energy range above E_l, where E_l is an input to the program. The Aurora calculation has a lower-energy limit of 0.5 keV. Although it is true that 0.5-keV incident electrons do not penetrate the atmosphere to the altitudes considered, energy is nevertheless deposited at these altitudes in the energy range below 0.5 keV by higher-energy electrons scattering down in energy. Hence the calculated results must be extrapolated down to $E_l = 0$ in order to obtain an estimate of the total energy deposited at any particular altitude.

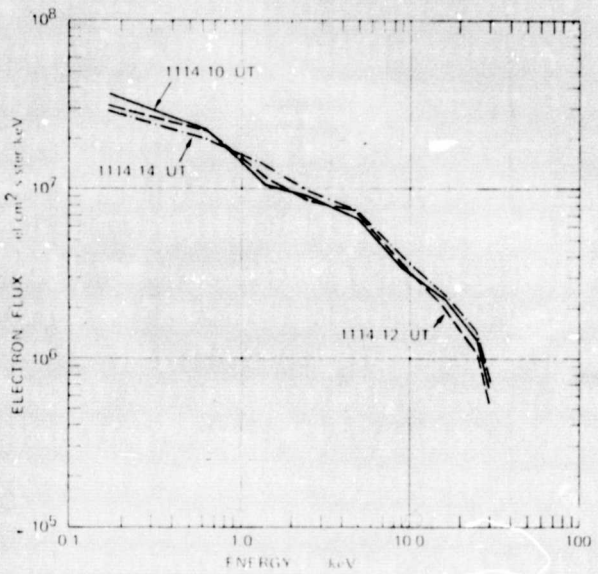

Fig. 8. Incident electron energy spectra determined from particle measurements on board the satellite 1971-089A during the coordinated radar-satellite experiment on January 27, 1972.

If we use the reasonable estimate of 35 eV of deposited electron energy corresponding, on the average, to the production of one electron-ion pair, the energy values provided by Aurora yield a direct estimate of the electron-ion production rate due to energetic electrons.

The Aurora calculation pertains only to production resulting from energetic electrons. A low intensity of energetic protons was observed to accompany the energetic electrons, and the total production taking place during auroral activity must include that due to energetic protons as well.

By using the method described by *Eather and Burrows*

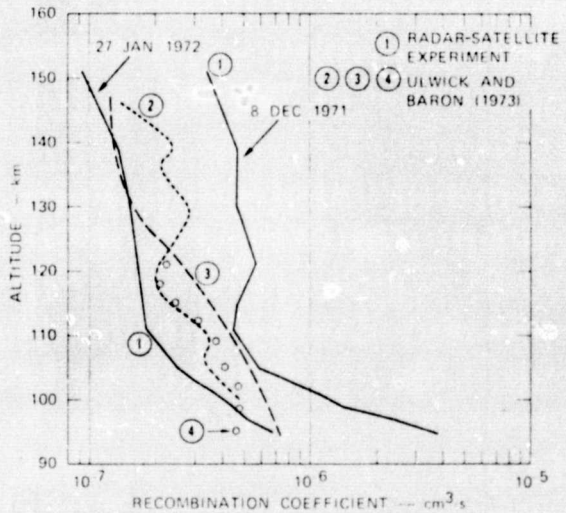

Fig. 9. Comparison of recombination coefficient profiles obtained from the radar-satellite experiment with profiles compiled by *Ulwick and Baron* [1973].

TABLE 1. Calculated Values of Electron-Caused Production, Proton-Caused Production, and Total Production at Various Altitudes

Altitude, km	December 8, 1971			January 27, 1972		
	Q_e	Q_p	Q_t	Q_e	Q_p	Q_t
151	2,660	10	2,670	1,155	250	1,405
139	4,560	13	4,573	2,193	380	2,573
130	7,450	21	7,471	3,875	640	4,515
121	11,250	28	11,280	7,305	930	8,235
115	13,850	34	13,880	11,150	1,120	12,270
111	15,050	37	15,090	14,900	1,250	16,150
105	13,450	13	13,460	20,460	800	21,260
103	11,680	10	11,690	22,200	480	22,680
101	9,350	8	9,360	23,400	160	23,560
99	6,140	6	6,150	23,100	0	23,100
97	4,030	3	4,030	21,500	0	21,500
95	2,780	0	2,780	17,250	0	17,250

Values are in electrons per cubic centimeter second.

[1966], electron-ion production profiles due solely to detected energetic protons were generated for the times 1331:07 to 1331:11 UT on December 8 and 1114:10 to 1114:14 UT on January 27, 1972. Total electron production was then taken to be the sum of the individual production rates due to energetic electrons and energetic protons. Table 1 lists values of electron-caused production Q_e, proton-caused production Q_p, and total production Q_t for each altitude at which the calculations were performed and for each of the coordinated measurements.

The overall uncertainties in Q_t are estimated to be less than 40%. These result from a combination of uncertainties in the absolute calibration of the sensors, counting statistics, deviations from isotropy, and calculational errors in the Aurora code. There are additional uncertainties resulting from spatial gradients in the particle fluxes. The latitudinal gradients in the observed fluxes are discussed later.

Applying the values of electron production from Table 1 and values of electron density from Figures 3 and 4 to (2) yields estimates of α.

The summarized results for both sets of coordinated measurements are given in Table 2 and are illustrated in Figure 9. It can be seen that the two α profiles varied with altitude in a similar manner but differed by a factor of about 3–4 over most of the altitude range, there being an increasing divergence below about 100 km.

Discussion

It is instructive to compare the results in Table 2 with results for α obtained by other means. Figure 9 compares the present results (curves labeled 1) with results taken from *Ulwick and Baron* [1973]. Curve 2 is based on data taken directly from an instrumented rocket launched on March 16, 1972, into an aurora from the Poker Flat rocket range near Chatanika. Curve 2 illustrates the results of electron production determined from energetic particle measurements and electron density determined from plasma frequency measurements. Curve 3 illustrates the results of using (2) along with rocket-mounted mass spectrometer measurements of $n(NO^+)$ and $n(O_2^+)$ [*Sherman et al.*, 1973], laboratory values for $\alpha(NO^+)$ and $\alpha(O_2^+)$ [*Biondi*, 1969], and a Cira (1965) mean temperature model. Curve 4 illustrates results obtained on February 24, 1972, by applying the 'probability distribution' method to incoherent scatter measurement data [*Baron*, 1972]. It can be seen that the results of January 27, 1972, agree quite well with those results obtained by other means and that the α profile obtained on December 8, 1971, seems to be comparatively high at all altitudes.

Figure 10, taken directly from *Cladis et al.* [1973], presents a compilation of α values obtained during auroral activity by a number of workers. In the altitude range 100–125 km, α values given in Figure 10 vary over a range greater than 1 order of

TABLE 2. Calculated Values of Total Production, Electron Density, and Effective Recombination Coefficient at Various Altitudes for the Radar-Satellite Experiments

Altitude, km	December 8, 1971			January 27, 1972		
	Q_t, el/cm^3 s x 10^3	N, el/cm^3 x 10^5	α, cm^3/s x 10^{-7}	Q_t, el/cm^3 s x 10^3	N, el/cm^3 x 10^5	α, cm^3/s x 10^{-7}
151	2.67	0.88	3.45	1.405	1.23	0.93
139	4.57	0.98	4.76	2.573	1.38	1.35
130	7.47	1.27	4.63	4.515	1.71	1.42
121	11.28	1.50	5.69	8.235	2.21	1.68
115	13.88	1.72	4.69	12.27	2.65	1.75
111	15.09	1.83	4.50	16.15	2.96	1.84
105	13.46	1.51	5.90	21.26	2.92	2.50
103	11.69	1.21	8.00	22.68	2.75	3.00
101	9.36	0.91	11.30	23.56	2.54	3.65
99	6.15	0.66	14.1	23.1	2.28	4.45
97	4.03	0.41	24.0	21.5	2.02	5.28
95	2.78	0.27	38.1	17.25	1.60	6.74